# INVESTIGATING THE EFFECTS OF COLLAGEN FIBRIL ALIGNMENTS ON HEPATOCELLULAR CARCINOMA CELLS

## SELİN OKTAY

Master's Thesis

Graduate School

Izmir University of Economics

Izmir

2022

# INVESTIGATING THE EFFECTS OF COLLAGEN FIBRIL ALIGNMENTS ON HEPATOCELLULAR CARCINOMA CELLS

**SELİN OKTAY**

A Thesis Submitted to

The Graduate School of Izmir University of Economics

Master's Program in Bioengineering Program

Izmir

2022

# ABSTRACT

## INVESTIGATING THE EFFECTS OF COLLAGEN FIBRIL ALIGNMENTS ON HEPATOCELLULAR CARCINOMA CELLS

Oktay, Selin

Master's Program in Bioengineering

Advisor: Asst. Prof. Dr. Burçak ALP

November, 2022

Collagen is a biological polymer that is frequently encountered in tissues and plays a key role, which has been the subject of many research from the past to the present. It has been proven that some diseases occur as a result of the change in the structure of this polymer due to biological and external factors, which is abundant in the structure of the extracellular matrix (ECM). It is thought that the collagen in the ECM structure interacts with cell groups such as endothelial and hepatocyte cells in liver fibrosis disease and induces some specific molecular signals, increasing vascularity and stiffness in the tissue and causing tumor formation. In this study, different collagen fibril alignments were simulated by electrospinning, magnetic force and mechanical force, and the behavior of hepatocellular carcinoma cells in these different fibril arrangements was investigated. The upregulation trend of Krt19, Hnf1a and Hnf4a genes of Huh-7 cells was observed on aligned collagen fibrils, suggesting that hepatocellular carcinoma cells would behave more aggressively in tumor development than random fibrils.

# ÖZET

## KOLAJEN FİBRİL HİZALANMASININ HEPATOSELÜLER KARSİNOM HÜCRELERİ ÜZERİNDEKİ ETKİLERİNİN İNCELENMESİ

Oktay**,** Selin

Biyomühendislik Yüksek Lisans Programı

Tez Danışmanı: Dr. Öğr. Üyesi Burçak ALP

Kasım, 2022

Geçmişten günümüze kadar birçok araştırmaya konu olan kolajen, dokularda sıklıkla rastlanan ve anahtar roller üstlenen bir biyolojik polimerdir. Ekstraselüler matriks (ESM) yapısında bol miktarda bulunan bu polimerin, biyolojik ve dış faktörler sebebiyle yapısının değişmesi sonucunda bazı hastalıkların ortaya çıktığı kanıtlanmıştır. ESM yapısındaki kolajenin karaciğer fibrozu hastalığında endotel ve hepatosit hücreleri gibi hücre gruplarıyla etkileşime girip bazı spesifik moleküler sinyalleri indüklemesiyle birlikte dokuda damarlanmayı ve sertliği arttırarak tümor oluşumuna sebep olduğu düşünülmektedir. Bu çalışmada farklı kolajen fibril hizalanmaları elektroeğirme, manyetik kuvvet ve mekaniksel kuvvet yaratılarak taklit edilip, bu farklı fibril düzenlerinde hepatoselüler karsinom hücrelerinin davranışları incelenmiştir. Hizalanmış kolajen fibrillerine ekilen Huh-7 hücrelerinin Krt19, Hnf1a ve Hnf4a genlerinde upregulasyona meyilli olduğu görülmüş, hepatoselüler karsinom hücrelerinin hizalanmış fibrillerde hizalanmamış olanlara göre tümor gelişiminde daha agresif davranacakları düşünülmüştür.

Anahtar Kelimeler: Kolajen, Karaciğer Fibrozu, Karaciğer Kanseri, Kolajen Fibril Hizalanması, Hepatoselüler Karsinom Hücreleri.

# ACKNOWLEDGEMENTS

# TABLE OF CONTENTS

# LIST OF TABLES

# LIST OF FIGURES

# CHAPTER 1: INTRODUCTION

## 1.1. Liver Diseases and Collagen

### 1.1.1. Molecular Structure and General Physiology of Liver

The liver in mammals has a key role in regulating and protecting the vital activities of living things. This organ, which has a complex vascular structure and cleans the blood from toxic substances, acts as a filter, making nutrient intake efficient, also undertakes vital functions for the immune system (Arias et al., 2020). Bile produced in the liver, providing the absorption of fat and some vitamins, it regulates the homeostasis in the body and has antibacterial properties for intestinal metabolism (Chiang and Ferrell, 2018). Known to have unique functions, this structure usually includes two cell types: hepatocytes and biliary cells (Arias et al., 2020). These cells regulate the structural, metabolic, and immunological activities of the living thing. The cells that support the immune system in the liver are specifically called Kupffer cells (KC) (Arias et al., 2020). In addition, hepatic stellate cells (HSC), which are silent in the healthy liver, store vitamin A after activation and contribute to the formation of the extracellular matrix (Tsuchida and Friedman, 2017). The liver has developed the ability of regeneration so that the living thing can continue its vital activities and return to a healthy form after injury. In this way, new cells quickly replace the dysfunctional cells that undergo necrosis and apoptosis, thereby minimizing damage to the liver (Diehl, 2002).

### 1.1.2. Liver Diseases and Cancer

While the liver has vital functions and duties in the living body, it loses essential functions by being damaged due to metabolic problems such as excessive alcohol use, viral infections (Hepatitis B and C), smoke, obesity, impaired glucose mechanism and fat accumulation. Diseases such as nonalcoholic steatohepatitis (NASH), primary biliary cholangitis (PBC), cholestasis, fibrosis and cirrhosis occur in the damaged liver (Bataller and Brenner, 2005; Henriksen and Møoller, 2004; Anwanwan et al., 2020). In ongoing chronic damage, a lot of liver diseases can result in hepatocellular carcinoma (HCC), a type of cancer, and may be fatal to the living things (Ringehan, McKeating and Protzer, 2017).

### 1.1.2.1. Liver Cancer and Current Treatment

According to the data published by the World Health Organization (WHO) in 2015, cancer is the leading cause of death worldwide. Turkey became one of the countries with the highest number of cancer cases with 116,710 cases in 2018 (WHO, 2018). At the same time, research as of 2018 shows liver cancer, which is the seventh cancer type with the highest mortality rate among different cancer types (Bray et al., 2018). Only 15% of patients with liver cancer regain their health because of appropriate treatment (Anwanwan et al., 2020). In addition to the high mortality rate of this disease, it is also associated with some psychological, sociological, and economic problems in the society.

Knowing the molecular pathways of liver cancer is particularly important in terms of determining the causes of the disease and appropriate treatment. As a result of the research, the following molecular signaling pathways were discovered for liver cancer: Nuclear factor kappa B (NF-KB) and c-jun-NH2 kinase (JNK) pathway stimulated by cytokines such as TNF-a produced by inflammatory cells, mitogen-activated protein kinase (MAPK) pathway, signal transducers and activators of transcription (STAT) pathway (Nikolaou, Sarris and Talianidis, 2013).

With the use of stem cell technology in cancer treatment, it is aimed to destroy the disease by targeting cell groups such as embryonic stem cell, periductal oval cell, ductal liver progenitor cell observed in liver cancer. For this purpose, research continues today with markers such as CD133, CD90, CD90, CD91, CD92 and epithelial cell adhesion molecule (EpCAM) (Sell and Leffert, 2008).

Only a few options are available for the treatment of liver cancer. These are immunotherapy, trans arterial chemoembolization (TACE) therapy, which is used for asymptomatic patients and has low efficacy, kinase inhibitor chemotherapeutic drugs such as sorafenib and regorafenib, which cause toxic effects in long-term use, and healthy liver transplantation to the patient (Sieghart et al, 2013; LiverTox, 2018). The use of these chemotherapeutic drugs in treatment is not advantageous due to the low availability and high side effects. In addition, patients' access to organ transplantation is extremely limited due to the lack of suitable donors, considerable risk and expensive.

### 1.1.2.2. Liver Fibrosis and Collagen
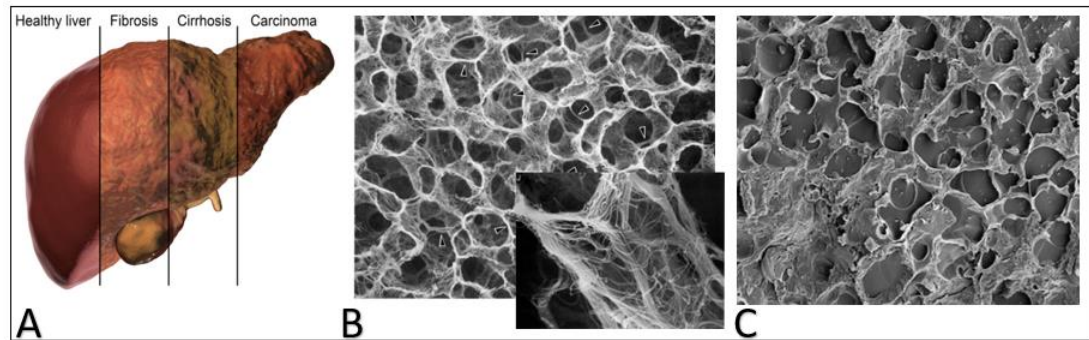


Figure 1. a) Representative cancer stages of the healthy liver. b) Scanning Electron Microscopy (SEM) image of collagen fibril network in healthy liver. c) SEM image of liver structure with cirrhosis (Source: Ohtani, 1992).

The liver is an essential organ for the living thing to maintain its vital activities. As explained above, due to some metabolic problems, this healthy structure deteriorates and leads to many diseases. Because of various injuries, parenchymal cells are activated and create an inflammatory response in the liver. When these inflammations become acute, regeneration in the liver fails and hepatocyte cells begin to produce extracellular matrix proteins such as fibrillar collagen for correct this injury (Bataller and Brenner, 2005). This behavior of hepatocyte cells is a normal process of wound healing. However, the production of fibronectin, elastin, laminin, and especially type I collagen is constantly repeated, and a large amount of extracellular matrix accumulates in the liver tissue (Bataller and Brenner, 2005). Inactive form of Hepatic stellate cells is activated by the contribution of Kupffer cells (KC) with the TGF-b molecular signal, inducing the production of tissue inhibitory metalloproteinases (TIMPs), and as a result, type I collagen begins to be produced too much in the damaged area (Iredale, Thompson and Henderson, 2013). Studies have shown that the accumulation of fibrillar collagen in the liver is highest in the portal areas and around the central vessels (Rouède et al., 2020; Gailhouste et al., 2010). As explained in detail above, disruption of the balance between matrix metalloproteinases (MMPs) that degrade extracellular matrix molecules and TIMPs that inhibit their induction leads to liver fibrosis (Rieder et al., 2007). The increase in the amount of accumulated collagen causes the progression of

liver fibrosis and hardening of the tissue (Brashear et al., 2021). In addition, the last stage of fibrosis is cirrhosis, and after this stage, the patient's recovery potential is seriously reduced (Figure 1) (Chen et al., 2019). Some researchers have argued that there is a direct correlation between collagen density and tumor formation (Provenzano et al., 2008). Based on this finding, "Failure to stop liver fibrosis can lead to cancer formation." comment can be made.

### 1.1.3. Collagen Molecular Structures, Alignment and Effect on Cells

The molecular structure of collagen is the "The Rich and Crick" model, which has been accepted in research since 1955. In this model, each peptide strand of the collagen molecule containing three polypeptide subunits. These subunits are mostly right-handed and has a triple helix structure (Okuyama et al., 2005; Guo and Kaufman, 2007). Collagen has a complex arrangement. It consists of the amino acid sequence identified by "Gly-X-Y". Each of the 3 residues starts with a Glycyl (Gly), and X and Y consist of Proline (Pro) and Hydroxyproline (Hyp), respectively. Many amino acids in the collagen structure come together to form α chains. The α chains come together with the help of hydrogen bonds to form the triple α helix structure, and in the meantime, the D-band region (67 nm) is formed which is a characteristic feature of collagen. These collagen fibrils form cluster with self-assembly and finally collagen fibers are created with a width of about 300 nm (Sorushanova et al., 2019).
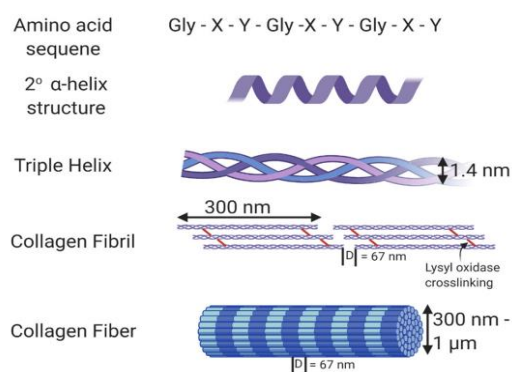


Figure 2. Structure of collagen (Source: Walimbe and Panitch, 2020).

One of the main components of the extracellular matrix is collagen molecules. Under suitable conditions, collagen molecules naturally develop a molecular architecture for have high tensile strength, according to the needs of the tissue in which they are located. This developed architecture is shaped according to

the laws of thermodynamics and the bond relations between them (Guo and Kaufman, 2007). Collagen molecules grow structurally and form the fibrous structure with the help of the mentioned factors (Figure 2). This fibrous structure, (also evident in tendon and ligament tissues) is regularly aligned in multiple layers in parallel form. While the alignment of collagen varies according to the tissue it is in, it is most irregular in the connective tissue (Holmes et al., 2001).

Simulating the environment of cell lines to ECM supports their growth, signaling and differentiation activities. At the same time, simulating the 3D ECM structure with hydrogels makes it easy to monitor the behavior of the cell in vitro. This 3D structure can be supported by fiber alignments. As a result of *in vivo* studies, it has been shown that collagen fibril alignment changes the wound healing process by inducing cell proliferation (Lee et al., 2006).

Collagen alignment configurations have an impact on the behavior of cells. Delaine-smith et al. (2014) produced collagen scaffolds with regular and randomly aligned fibrils. The researchers cultured human fibroblast cells on the collagen scaffolds they had produced. They demonstrated that cells with regular alignment have greater elongation, migration capacity, and collagen production in a collagen scaffold (Figure 3) (Delaine-smith et al., 2014). In addition, Liu et al. (2015) cultured stem cells on the scaffold with regularly aligned collagen fibrils and then they argued that the gene expression of these cells increased (Liu et al., 2015).
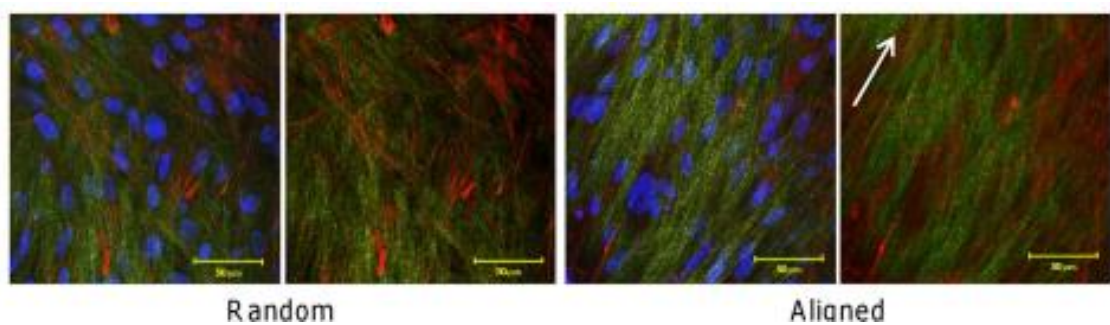


Figure 3. Human fibroblast cells cultured for 21 days were imaged using the second harmonic generation (SHG) method at 800 nm on the collagen scaffold with random fibril alignment and the regular fibril alignment (Source: Delaine-smith et al., 2014).

### 1.1.4. Collagen Density and Alignment in the Liver

As mentioned earlier, collagen deposition in liver scar tissue contributes more to the development of fibrosis than other extracellular matrix proteins (Chen et al., 2014). Studies have reported that mostly type I and type III collagen accumulate in fibrous tissue, however a small amount of type IV collagen observe (Iredale, Thompson and Henderson, 2013). Lin et al. (2013) developed fibrosis in tendon tissues with regular and parallel collagen alignment, and they proved that type 1 collagen predominately accumulates in fibrosis (Lin et al., 2013).

Few studies have interpreted the relationship between liver fibrosis and collagen alignment. In the same study by Lin et al. (2013), they observed that regular alignment structure of collagen had a more random configuration during fibrosis (Lin et al., 2013). In addition, Rouède et al. (2020) made a classification by investigating collagen alignment structures in different tissues. The researchers wanted to look at the collagen alignment architecture in liver fibrosis and developed an imaging model (Figure 4). They associated extracellular matrix deposition during fibrosis and associated liver stiffness with fibrosis (Rouède et al., 2020).
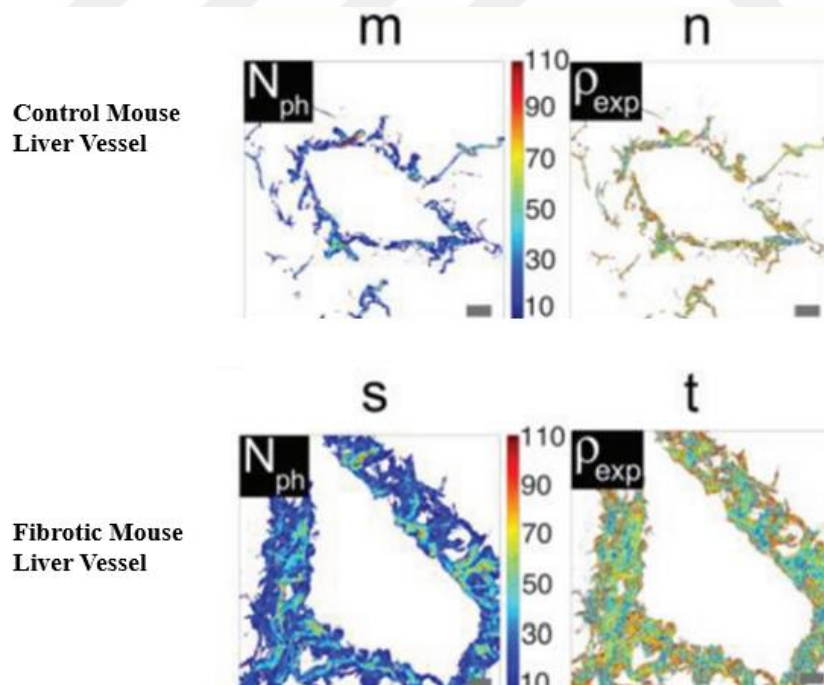


Figure 4. Comparison of healthy mouse liver and fibrosis mouse liver by polarization-dependent second harmonic generation (P-SHG) method by mathematical model. (First column: m, s) Typical 512×512 pixels SHG image

obtained from average of the P-SHG stack. The color bar represents the mean photons number per pixel *Nph*. Scale bar is 10 μm. (Second column: n, t) Map of the experimental anisotropy parameter *ρexp.* In the image represented by 's' in the fibrous mouse liver, more stiffness was found in the image represented by the 'm' in the healthy mouse liver (Source: Rouède et al., 2020).

The relationship between regularly aligned collagen fibrils and cancer formation was demonstrated by Riching et al. (2014). While collagen density increases in breast cancer, tissue stiffness also increases. Knowing this, the researchers wanted to include the collagen fibrils in this study. As a result of this study, they proved that collagen fibrils with more regular alignment cause more tissue stiffness and therefore they are more tend to cancer formation (Figure 5) (Riching et al., 2014).
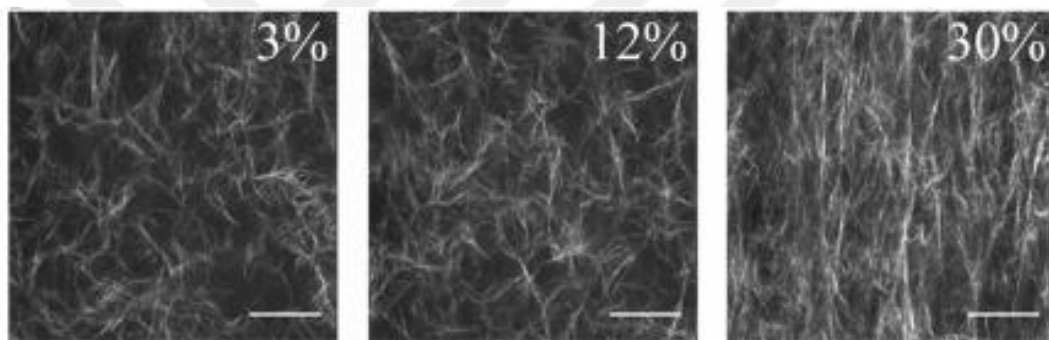


Figure 5. While tension and collagen density increase in the collagen gel, the alignment in the fibrils becomes more regular (SHG image) (Source: Riching et al., 2014).

### 1.1.5. Cell Models of Liver and Liver Fibrosis

In vitro cell models are used as an alternative to animal models for mimic and study liver diseases. Because while studies on animal models have been successful, the same studies have not been significantly effective on humans (Sacchi, Bansal and Rouwkema, 2020). Most studies using liver fibrosis modeling methods examine drug resistance, chemicals, and specific metabolic pathways. These models are generally; Simple 2-dimensional mono-layer cultures in which HSCs are cultivated classically used in most studies, 3-dimensional HSC spheroid tissue cultures and organoids, which can mimic disease more realistically and more advantageously compared to other cell models. Lastly microfluidic bioreactors that co-cultures using HSC and

hepatocytes combined models. These are high cost and less reliable (Yoon et al., 2015).

2D standard cell models cannot fully model every stage of liver fibrosis and they cannot model the cell behaviors in fibrosis (Sacchi, Bansal and Rouwkema, 2020). In addition, 3D liver fibrosis models created by the hanging drop method can be differentiated at the desired size and cell level. Also, these models completely imitate the fibrosis environment for up to 5 weeks (Bell et al., 2016). Organoids contain more cell types than classical 3D models. They are one of the most effective methods for modeling fibrosis because they can better mimic the cellular architecture and organization of tissue (Sacchi, Bansal and Rouwkema, 2020). Researchers have developed an organoid that mimics human lung tissue. They have proven that this method is effective by successfully modeling Idiopathic Pulmonary Fibrosis (IPF) (Wilkinson et al., 2016).

### 1.1.6. Collagen and Molecular Behavior of The Cell

The interaction of collagen with cells is important for understanding many biological mechanisms. In this way, it can be predicted how this protein affects cells and how it affects the proliferation and differentiation of cells. The mechanism of interaction generally works like this: Specific cell surface receptors help to transmit signals of cells to ECM proteins bi-directionally. Thanks to these receptors, it is easier for cells to bind to proteins. The binding of collagen to 5 different cell receptors and inducing interaction allows the emergence of different physiological functions (Elango et al., 2022). Researchers have proven that integrins and immunoglobulin-like receptors (Glycoprotein VI, Osteoclast-associated receptor (OSCAR)) use collagen as a ligand (Briesewitz, Epstein, and Marcantonio, 1993). Collagen binding integrins are classified as alpha 10 beta 1 ($\alpha10\beta1$), alpha 1 beta 1 ($\alpha1\beta1$), alpha 2 beta 1 ($\alpha2\beta1$), and alpha 11 beta 1 ($\alpha11\beta1$). Mostly $\alpha2\beta1$ integrin specifically bind to type 1 and type 3 collagen. These integrins induce remodeling through collagen in the wound healing process, increase the cell proliferation and collagen synthesis. As a result of the interaction of integrin with collagen, Mitogen-activated Protein Kinases (MAPK) signal is induced which initiates cell proliferation, and skin regeneration begins with the activation of Tyr-397 signal, which is involved in fibroblast differentiation (Elango et al., 2022). And also, it has been proven that

cancer formation is induced by increasing signals in hepatocyte cells and integrin expression in fibrous liver (Carloni et al., 2001). Glycoprotein VI binds to the glycine, proline and hydroxyproline amino acid sequences of collagen, activating integrins and performing signal communication (Labrador et al., 2001). The OSCAR receptor stimulates T cells, calcium molecular signal and activates them to which collagen binds. In this way osteoclast cells grow by signal transducer and activator of transcription 3 (STAT3) pathway (Zhou et al., 2016). Collagen also binds to Receptor tyrosine kinases (DDR), LAIR-1, and uPARAP/Endo180 receptors in biological cells (Elango et al., 2022). The development of organs is induced by type 1 collagen that binds to DDR (Shrivastava et al., 1997). Fibrillary collagen bound by DDR2 increases gene expression in cells for extracellular matrix deposition via the jun N-terminal kinases (JNK)/MAPK pathway and is effective for the cell to decide whether to undergo apoptosis (Ozaki et al., 2011). In pulmonary fibrosis studies, they proved that disease can be prevented by using the collagen and DDR receptor relationship to transform lung fibroblast cells into myofibroblast cells (Gadiya and Chakraborty, 2018). LAIR-1 allows peptide and collagen Gly-Pro-Hyp sequence to interact that induced by collagen triple helix (Meyaard, 2008). Collagen interacting with this receptor creates an effective defense for the immune system. Through the interaction, activity of natural killer (NK) cells is downregulated (Elango et al., 2022). The uPARAP/Endo180 receptor induces adhesion of fibroblast cells to collagen, thereby affecting cell adhesion, migration and proliferation on the fibrillar collagen matrix (Engelholm et al., 2003).

Collagen is also found in the vascular system. During vessel maturation, collagen fibrils become aligned and stimulate endothelial cells, thus migration is accelerated. Along with collagen alignment, signals between endothelial cells and the environment are induced via focal adhesion kinase (FAK), myosin II and Rho-associated protein kinase (ROCK) (Figure 6). As a result of this induction, MAPK and phosphoinositide 3-kinase (PI3K) mechanisms are activated and vessel formation or differentiation is activated (McCoy et al., 2018). Researchers have proven that fibrotic tissues are close to the vessel area (Rouède et al., 2020). In addition, vascular development is affected by the alignment of collagen fibrils and the relationship of endothelial cells at the molecular level (McCoy et al., 2018).
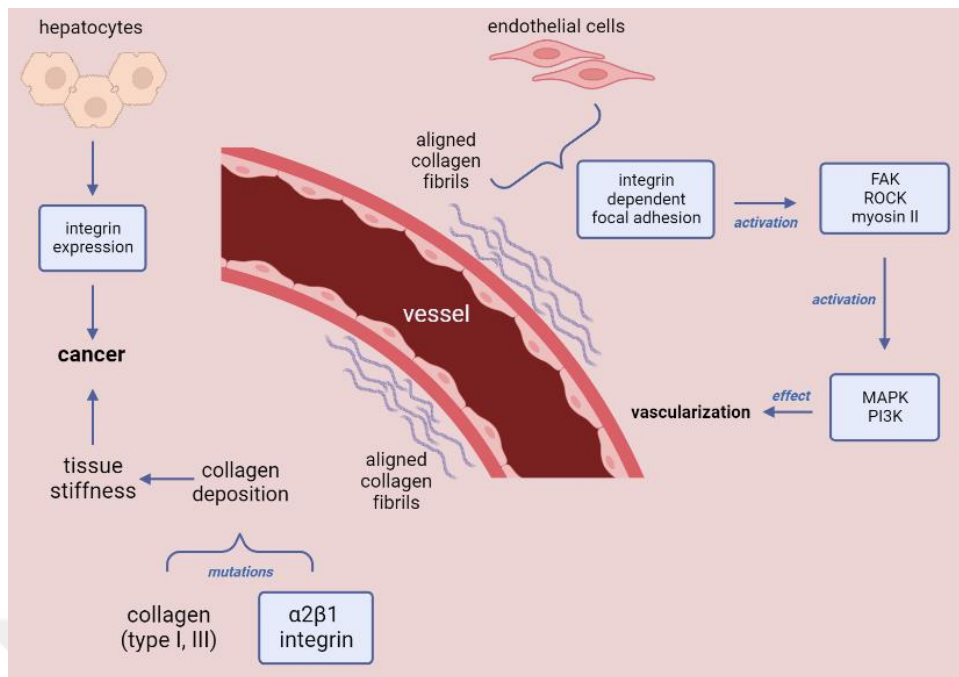
Figure 6. Schematic representation of the relationship of endothelial cells and aligned collagen fibrils with vascularization and the cancer formation as a result of integrin expressions in hepatocyte cells and mutations in collagen-integrin interaction.

As a result of the interaction of the cells embedded in the collagen gel with integrin signals, it has been revealed that the ECM-like structure affects the properties of cells such as differentiation and growth. The cytoskeleton properties of the cell may be altered by the expression of integrin in the collagen gel and the effect of this expression on other molecular pathways. It was proved that integrins were more expressed in 3D fibroblast cultures like collagen gels, their elongation increased, and they developed focal adhesion by inducing focal adhesion kinase signals (FAK) (DeMali, Wennerberg and Burridge, 2003). Cells attached to the ECM can induce changes in gene expression by stimulating other molecular pathways with integrin signals (Lv et al., 2015). In addition, integrin association with ECM proteins induces actin and actin-binding proteins and allowing proteins to interact with the cytoskeleton. It has been proven that the behavior of cells during integrin expression affects the stiffness of ECM structure by contracting collagen fibrils (Hocking, Sottile and Langenbach, 2000).

*1.2. Collagen Fibril Alignment*

As mentioned before, collagen fibril alignment is an important parameter to create a model for diseases and to observe the behavior of healthy cells and cancerous cells in structures with high collagen density, such as the liver. One of these diseases is liver fibrosis. Hepatic fibrosis is a disease that occurs as a result of unbalanced accumulation of fibrillar components in the liver and has a high probability of developing cancer in the later stages. As a result of fibrillar component deposition, disturbances in fibril arrangement were observed (Gailhouste et al., 2010). At the same time, researchers have proven that tumor growth increases with disruption of collagen fibril alignment in studies to monitor the progression of breast cancer (Riching et al., 2014). For many years, researchers have used many methods to change the arrangement of collagen fibrils and also to study the effects of collagen fibril alignment on diseases. Among these methods, there are frequently used electrospinning, interfering with the fibril arrangement with ultrasound waves and mechanical methods. Nowadays these methods are still used, and they are developing rapidly.

*1.2.1. Electrospinning*

The electrospinning method (Figure 7), designed in the 20th century, is a system that creates small-sized fibers in the desired size and configuration from a polymer solution (Buttafoco et al., 2006). Many studies have been carried out using the electrospinning method with extracellular matrix polysaccharides such as chitosan, cellulose, and proteins such as collagen and fibrin etc. Especially by combining collagen and synthetic or natural polymers are very common for wound dressing and scaffold applications with electrospinning method (Keirouz et al., 2020). Researchers formed the PCL-collagen scaffold by electrospinning and examined the effect of fibril alignments on fibroblast cells in this scaffold. They reported that as the order of fibril alignment increased, wound healing accelerated in rat (Kim and Kim, 2018).

This method works as follows: It is aimed that the polymer solution reaches target point and collects there with the help of a needle. This target point is designed according to the purpose of the study. The target can be a grounded plate or a

grounded rotating drum system. Voltage must be applied to the system for the solution to reach its target point. An electric field is created between the polymer solution and the positively charged target, and the appropriate voltage amount is given to the system. The electric field strength dominates the surface tension in the polymer solution. A jet formation is observed at the tip of the needle containing the polymer solution because of the created load imbalance. During jet moves towards to target, solvent of polymer solution evaporates, and it creates fibril-like structures. While the process continues, the number of dry fibrils in the target increase (Boland et al., 2004; Matthews et al., 2002). While the fibrils are randomly aligned by using a stationary target, the fibrils are regularly aligned by a rotating drum system (Buttafoco et al., 2006).
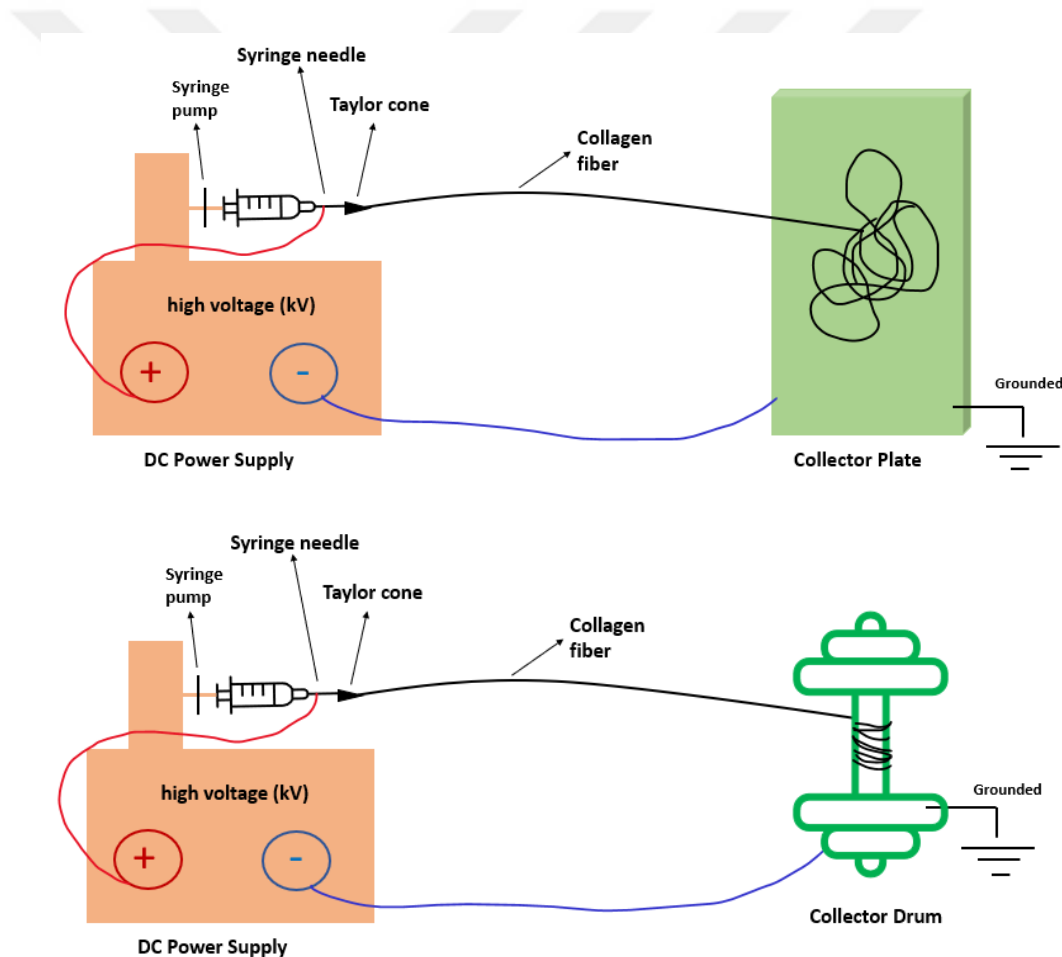


Figure 7. Representative image of electrospinning process with stationary collector and rotating drum collector.

### *1.2.1.1. Electrospinning of Collagen*

The collagen is a polymer with a fibril structure. It is a very suitable protein for use in tissue engineering applications. Nano size collagen fibers better mimic tissue and are preferred by researchers. It is very popular for use in wound dressings and drug delivery studies. Electrospinning method has been used for a long time to form collagen fibers at the nanometer level (Buttafoco et al., 2006). With this method, it is possible to produce fibrils in the desired three-dimensional structure. It is also quite easy to manipulate the chemical and biological content of the fibers (Matthews et al., 2002). Collagen fibers produced to be used as scaffolds in clinical applications must be biocompatible. Knowing the importance of this, researchers have been working for many years to produce a more biocompatible, biodegradable, non-toxic, inexpensive scaffold that better mimics natural collagen fibrils.

Electrospinning is a suitable method to mimic the collagen fibril structure. Researchers said that for collagen electrospinning, polymer chains must first be broken with the help of suitable solvent (Szeland et al., 2018). Simpson et al. (2011) exactly imitated natural collagen fibril patterns and alpha chains by electrospinning method (Figure 8). This result proved that the collagen fibers broken with the appropriate solvent were reassembled by electrospinning method. They also showed that the size of the fibers produced with the help of this method was similar to the natural collagen fibers (Simpson et al., 2011).
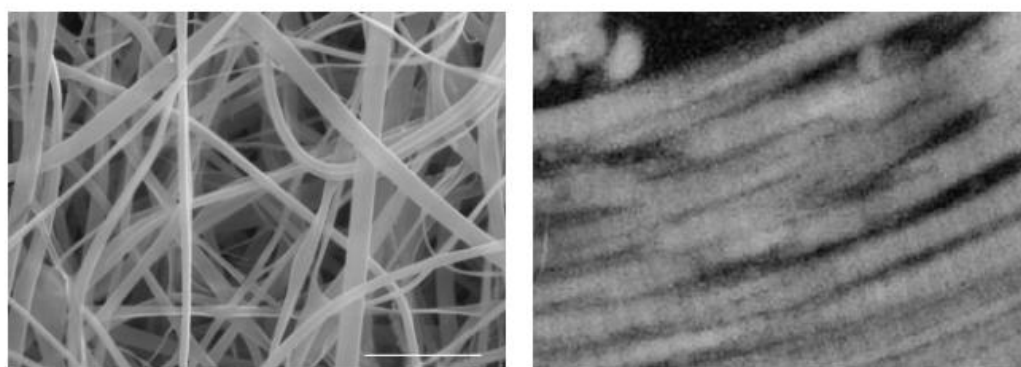


Figure 8. Representative (a) scanning electron and (b) transmission electron micrographs of electrospun collagen. Scale bar in (a) = 10 μm and (b) = 100 nm (Source: Simpson et al., 2011).

### 1.2.2. Ultrasound Waves and Alignment

The sounds with frequency higher than 20 kHz are called ultrasound (Song et al., 2018). It has been reported in the literature that ultrasound has the ability to create mechanical force and also interferes with the structure of collagen fibrils by releasing heat. They also stated that the application of ultrasound to the collagen fibrils reduces the fibril size with flow and increases the fibrinolytic effect (Braaten, Goss, and Francis, 1997). Garvin et al. (2013) formed a collagen gel and exposed it to 1 MHz ultrasound for investigate mechanical, thermal, and fibrillar properties. As a result, they reported that the gel contained shorter and thinner fibrils, and the collagen gel stiffness was high. Because of temperature conditions affect collagen polymerization, the heat generated by ultrasound indirectly affected the fibrils in the collagen gel (Garvin et al., 2013). Based on this information, it is concluded that collagen fibers can be changed by applied ultrasound.

In addition, a method such as magnetic alignment has been reported to mimic collagen fibril alignment in tissues. While collagen formed a gel, creating a magnetic field affected the alignment of the fibrils. When a magnetic field is applied to the gel, the fibrils are aligned perpendicularly. A magnetic field was applied to Schwann cells cultured in collagen gel for 2 hours. these cells were seen to align with collagen fibrils, which were aligned via the magnetic field (Eguchi, Ogiue-Ikeda and Ueno 2003).

### 1.2.3. Applied Force and Alignment

Changing the collagen fibril arrangement is useful when building models to observe cell behavior. How collagen gels respond to mechanical forces is one of the emerging research topics of recent times. Researchers used fibroblast cells to investigate the response of collagen gels to mechanical forces. The aim here is to model the skin and also to understand how cells will respond to aligned collagen fibrils. With the force released by contraction, fibroblast cells differentiate into myofibroblast cells faster. In addition to cell-cell signals and cell-collagen interaction, external factors also affect cells and can change their actions. While fibroblast cells are protected from environmental loads on the skin, they can create force and change collagen alignment when interacting with collagen (Brown, 2013).

It has been stated that as a result of tensile loads to the cells in collagen gels, the cells affect the structure of the gel. This also applies to the opposite situation. In summary, the interaction between collagen fibril alignment and fibroblast cells is affected by the tensile load parameter (Porter et al., 1998). The interaction between collagen gels applied mechanical one-dimensional strain and fibroblasts, muscle cells was investigated. It was stated that collagen and cell alignment increased up to 50% by applying strain (Girton, Barocas and Tranquillo, 2002).

In addition to the previously mentioned alignment methods, it is mentioned in the literature that mechanical force can be created in a simpler way. The researchers added skeletal muscle myoblast cell line into the collagen gel. They put the solution containing cells and collagen gel into capillary tube molds. Then they centrifuged the solution at 1000 rpm for 5 minutes. The aim here was to increase the density of the collagen gel by reducing the volume of the collagen gel with continuous cyclic force in the centrifuge. Thus, thanks to the mechanical stress, the cells were more evenly distributed in the dense collagen gel (Okano and Matsuda, 1998). It was thought that with this force, the fibril patterns in the collagen gel could also be changed. It was interpreted that the constant mechanical force applied during collagen gel formation could create a new method for fibril alignment.

### 1.3. The Aim of Study

Nowadays, appropriate imitation of natural tissue has been important in terms of the source of research. The better we can imitate natural tissue, the better we can understand it. We need tissue models to learn how diseases develop, how to stop them, and which parameters are important for the disease.

Based on the previously reported information, hepatocellular carcinoma cells (HCC) are malignant cells in the liver that have abnormal appearances. It is known that the number of these cells increases in the liver with cirrhosis, which develops with the continuous inflammation in liver fibrosis. With constantly developing inflammation, the DNA damage of the cells increases with oxidative stress and allows HCCs to develop and spread further. Hepatocytes can be found in the liver as stem cells that can undertake various functions. Instead of increasing the cell proliferation rate, hepatocytes try to minimize liver damage by copying themselves

(Alison, 2005). Researchers reported that while the proliferation rate of hepatocyte cells decreases in chronic hepatitis disease, the activation of stem cells (hepatic progenitor cells) in the intrahepatic region begins at the same time (Yang et al., 2004). Stem cell group called oval cells in the Hering canals of liver are cells that can differentiate into hepatocytes. Researchers aiming to see hepatic stem cells with cytokeratin-19 in necrotic liver proved that these cells spread from portal tracts to Hering canals and changed into hepatocyte cells (Theise et al., 1999). Alignment of collagen fibrils around portal tracts in liver fibrosis has been mentioned before (Rouède et al., 2020). Collagen accumulation increases around the portal tracts as a result of the interaction of collagen molecules with endothelial and hepatocyte cells, with impaired integrin signals due to internal and external factors. Meanwhile, abnormal expression of the PI3K molecular pathway with abnormal integrin signals supports the formation and proliferation of tumor cells. With the accumulation of collagen fibrils, the stiffness seen around the vessel also increases, supporting the abnormal behavior of the tissue and increasing the prognosis of the disease. Healthy cells affected by molecular pathways cause cancer formation in the region where stiffness increases as a result of this abnormal collagen behavior and abnormal signals. With the increase in collagen fibril alignment, it is expected that the cytoskeleton structure of hepatocyte cells interacting with the collagen molecule will change, while the network of the cell will be changed. It is expected that the hepatic progenitor cell characteristics will change, and the cancer gene expressions of hepatocellular carcinoma will increase with the intervention of the cell structure.

In this study, collagen fibrils were produced in different arrangements as random and aligned. Collagen gels were used to create 3D environment for hepatocellular carcinoma cells and to examine their behavior in the gel. It was investigated how the behavior of *Huh-7* cells changed in different collagen fibril arrangement. In this way, it was desired to comment on the effect of different collagen fibril alignment on liver cancer cells.

16

# CHAPTER 2: MATERIALS AND METHODS

## *2.1. Collagen Extraction*

Collagen extraction method was taken from the literature and has been modified (Ju et al., 2020). For collagen production, bovine tendons were used with acid-solubilized extraction method. Bovine tendons were obtained from local butchers in Izmir, Turkey. Unless otherwise stated, all chemicals used were obtained from Sigma Aldrich Co. Before starting the extraction, all bovine tendons were cut 2 cm thick and washed with distilled water. The chemical rates and times of all pretreatment and acid solubilized extraction are described in Table 1.

### *2.1.1. Pretreatment*

The pretreatment method was used to break intermolecular covalent bonds between collagen molecules before the acid-solubilized extraction. Firstly, the tendons were pretreated with 0.05 M (hydroxymethyl) aminomethane (TRIS) and 1 M sodium chloride (NaCl) at a ratio of 1/20 (w/v). The 8,8 grams of bovine tendon was taken for preparation of sample A. For sample B, the 12,8 grams of bovine tendon pieces were taken, chemicals and bovine tendon ratio were set to 1/20 (w/v). The tendons and pretreatment solutions were left on the magnetic stirrer at 4 $^o$C for 48 hours. The chemicals were changed twice a day. Secondly, 4 %, 250 ml of Ethylenediaminetetraacetic acid (EDTA; 4,2 pH) was prepared for pretreatment solution of sample C and D. The 1 M and 5 M sodium hydroxide (NaOH) were added slowly to make its pH value 7,4. A pH meter was used at each stage for measurement. The 10 grams of bovine tendons were obtained for sample C and D, and they were kept in 400 ml of EDTA solution. Pretreatment took 24 hours for C and 72 hours for D.

### *2.1.2. Acid-Solubilized Extraction*

After the TRIS and NaCl pretreatment, sample A and B were left in 0,83 M acetic acid solution for 36 hours. At the end of the procedure, the tendon solution was centrifuged for 10 minutes with 10000 rpm. The precipitate was collected, crushed, and added to 0,5 M acetic acid. The resulting collagen sample were mixed in a magnetic stirrer until completely dissolved. Sample C was removed from the

EDTA and mixed with 0.2 M acetic acid 1/10 (w/v) in a magnetic stirrer for 48 hours at 4 °C. The supernatant was discarded after centrifugation of the solution, and the pellet was stirred in 0.2 M acetic acid for 2 days. After EDTA pretreatment, the sample C and D tendons were removed from the solution and mixed with 0.2 M acetic acid 1/10 (w/v) in a magnetic stirrer for 2 days. The supernatant was discarded after centrifugation of the solution, and the pellet was stirred in 0.2 M acetic acid for 2 days. The centrifugation procedure of sample C was followed for sample D.

Table 1. Different pre-treatment and acid extraction methods of bovine tendons for different densities.

| Sample Name | A | B | C | D |
|---|---|---|---|---|
| Weight of Tendons (g) | 8,8 | 12,8 | 10 | 10 |
| Pre-treatment (w/v) (g/ml) | TRIS and NaCl (1/20) | TRIS and NaCl (1/20) | EDTA and Distilled Water (1/10) | EDTA and Distilled Water (1/10) |
| Acetic Acid Treatment (w/v) (g/ml) | 0,5 M (1/20) | 0,5 M (1/20) | 0,2 M (1/10) | 0,2 M (1/10) |

### 2.1.3. Dialysis

In sample C collagen solution, dialysis was used as the post extraction method. Dialysis method was performed with 0.5 M acetic acid to remove neutral salts and other proteins from the collagen solution. In particular, ionic migration is initiated between the dialysis tube and the acidic environment to remove the precipitated salts from the collagen solution (Matinong et al., 2022). The dialysis tube (Sigma Aldrich) was passed through distilled water to reach the appropriate volume. The bovine tendons were filtered and placed in dialysis tube. The samples were kept in 0.5 M acetic acid for 2 days at 4 °C.

### 2.1.4. SDS-Page

Sodium dodecyl sulfate–polyacrylamide gel electrophoresis (SDS-Page) technique was applied to control the collagen purity in the content of sample D used in cell culture. First of all, resolving gel and stacking gel were prepared for the experiment. For resolving gel, 12,1 g 2-Amino-2-(hydroxymethyl)-1,3-propanediol (Trizma-Base) was dissolved in 80 ml distilled water and the pH value was brought to 8,8 with 5 M hydrochloric acid (HCl). Distilled water was added to make the final volume to 100 ml. For stacking gel, 12,1 g Trizma-Base was dissolved in 80 ml distilled water. The pH value of stacking gel was adjusted 6,8 with 5 M HCl. 30 ml 40 % acrylamide/bis-acrylamide solution was taken, and 10 ml distilled water was added to make a 30 % acrylamide solution. 1 g of SDS was dissolved in 10 ml distilled water and N,N,N',N'-Tetramethyl ethylenediamine (TEMED) was used as bought. For preparing to 10% acrylamide gel for resolving gel, 1,280 ml distilled water, 1,67 ml 30 % acrylamide, 1,95 ml 1 M Tris-HCl (pH 8.8), 50 µl 10 % SDS, 50 µl 10 %APS and 5 µl TEMED were mixed. This gel was poured in between gel plates with 1 ml pipette and 1 ml ethyl alcohol (EtOH) was poured at the top of the gel to smoothen the gel. When gel was set, EtOH was removed from the top with a paper towel. Then stacking gel solution was prepared as 3 ml. For this solution, 1,317 ml distilled water, 498 µl 30 % acrylamide mix, 1,125 µl 1 M Tris (pH 6,8), 30 µl 10 % SDS, 30 µl 10 % APS and 3 µl TEMED were mixed and poured the machine. The comb was inserted at the top of gel and waited for 15 min. For sample preparation, 7 µl β-Mercaptoethanol was added into 1 ml 5X loading dye containing 1 mg Bromophenol Blue (1 % (w/v)), 0,5 ml glycerol (50 % (w/v)), 80 mg SDS (8 % (w/v)), 0,25 ml Tris-Cl (250 mM, pH 6,8) and 0,243 ml distilled water. The 4 units of sample and 1 unit of 5X SDS loading dye were loaded and total volume was around 50 µl. The 2x, x, 0,75x, 0,5x and 0,25x dilutions of collagen sample D were used. Samples were boiled at 95 $^{\circ}$ C for 5-10 min and let it reach back to room temperature before loading on a gel. The 1 liter of running buffer was prepared. 30,275 g 2 Trizma-Base, 144 g glycine, and 50 ml 20 % SDS were mixed and bring the volume to 1 liter. Until the samples were passes the stacking gel, the gel was run slowly like at 60 kV for 90 min. Then the speed was increased to 120 kV for 90 min. For staining process, the gel was removed from the set-up carefully and rinsed with distilled water. Two different solutions were prepared as solution 1 (50 % EtOH and

10 % acetic acid) and solution 2 (5 % EtOH and 7,5 % acetic acid). The gel was transferred to staining box with 50 ml solution 1 and heated in microwave for 30 sec. Then the gel was cooled in shaker for 5 min. Solution 1 was removed from the gel and 50 ml solution 2 was added. At the same time, 250-500 µl Comassie mix (0,25 % Coomasie Brillant Blue R-250 in 95 % EtOH) was directly added to solution 2 in staining box. The gel was heated in microwave for 30 sec and cooled on shaker for 5 min. Bands were appeared on this time. After 1 hour, image was obtained, and gel was left in stain overnight on the shaking. Photographs of the bands were taken after 24 hours.

### 2.1.5. UV-Visible Spectroscopy

UV-Vis Spectroscopy (PerkinElmer Lambda 750 UV/VIS/NIR Spectrometer) was performed to find the concentration of collagen samples obtained from different amount of bovine tendons. 0.5 M acetic acid was used as a blank for analysis. According to Ferraro et al. (2017), collagen formed a peak at 280 nm. Based on this information, the 280 nm wavelength was used for analysis of sample A, B, C and D. 0,7 ml of A and B collagen solutions were taken from each sample, and they were put in the 0,7 ml quartz cuvettes (pathlength = 10 mm) (IsoLab). Also 3,5 ml of C and D collagen solution were taken for analysis, and they were placed in 3,5 ml standard quartz cuvettes (pathlength = 10 mm). At the same time, company's collagen (2 mg/ml) was analyzed as a reference value for determining concentrations of samples. A graph was obtained from the samples that absorbance was measured. Concentration of this collagen was compared with the sample A, B, C, and D. The concentration of the bovine tendon collagen samples was calculated from the obtained data.

### 2.1.6. Yield Calculation

The yield calculation of the extracted collagen was done using the following equation (Ju et al., 2020):

The yield of Acid-Solubilized Extraction (%) = (W2/W1) × 100%. (1)

W2 is the dry weight of the extracted collagen and W1 is the dry weight of the bovine tendon used. The lyophilization method was used for 24 hours to reach the dry weight of the samples.

## 2.2. Collagen Gel

### 2.2.1. Formation

The process of collagen gel was produced from extracted bovine tendon collagen (Levis, Brown, and Daniels, 2010). This procedure was used for A, B, C and D collagen samples. Firstly, 4 ml of collagen solution and 0.5 ml of 10x Minimum Essential Medium Eagle (MEM) (Sigma Aldrich) were gently mixed. 5 M and 1 M NaOH was slowly added to the collagen until color change was observed for neutralizing the solution (Figure 9). These collagen gels were poured into 2 types of molds with 3,5 cm x 2,5 cm x 0,5 cm and 32 mm x 32 mm x 150 mm. They were placed in a 5% $CO_2$ incubator at 37 °C for 30 minutes because to complete the gelation process.
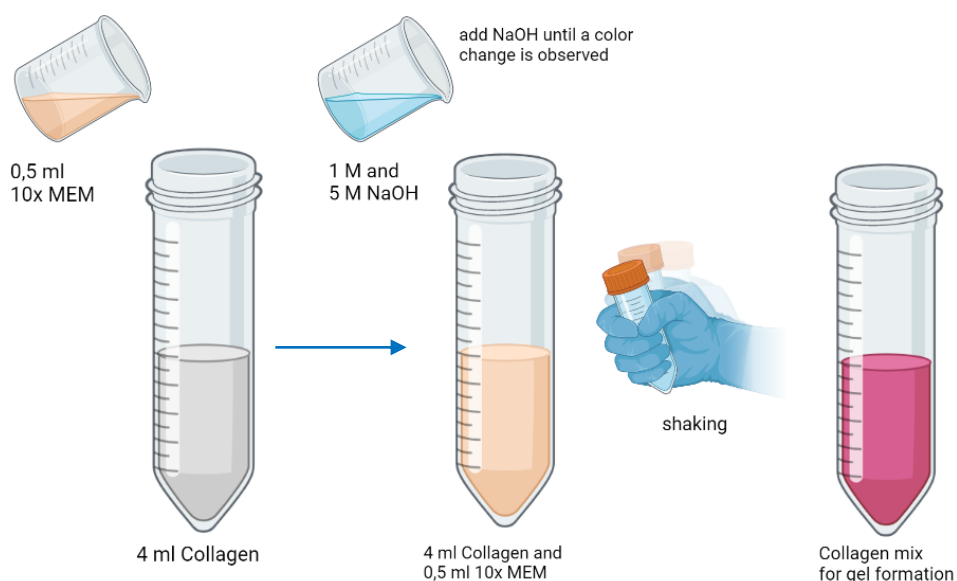


Figure 9. Collagen gel formation process.

### 2.2.2. Plastic-Compression of Collagen Gel

Plastic compression method (Figure 10) was applied to improve the mechanical properties of the produced collagen gels (Levis, Brown, and Daniels, 2010). The collagen gels were removed from the molds, and they were placed

between 2 pieces of nylon mesh. They were exposed to compression for 5 minutes with the help of a 120-g flat block. The gels obtained at the end of the plastic compression procedure was gently lifted over the nylon mesh.
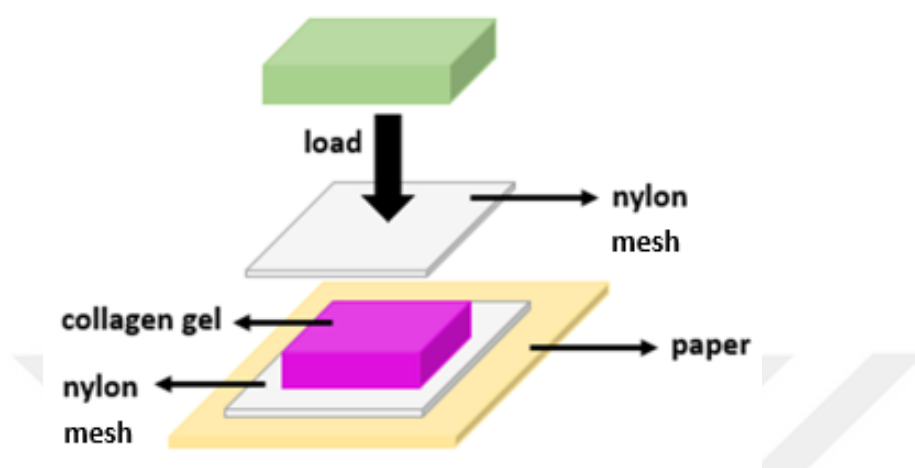


Figure 10. Representative image of plastic compression method of collagen gel.

### 2.2.3. Self-Compression of Collagen Gel

For the self-compression procedure standard collagen gel formation process was applied. Gels were placed on filter paper. The liquid in the gel was expected to go away on its own. The procedure continued for 20 minutes, and weight of the gel was measured with a precision balance (Shimadzu Corporation, Japan) every 2 minutes.

### 2.2.4. Physical Characterization

### 2.2.4.1. Length, Height, and Thickness of Collagen Gels

The thickness of the collagen gels was measured using a digital micrometer (The Mitutoyo, MDC-Lite Digimatic, Japan). The lengths and heights of the gels were measured with a digital caliper (6 in). Measurements were taken from 3 different points of the gels and the average thickness was calculated. The thickness of the collagen gels was measured in dry conditions after plastic-compression method and self-compression method.

### *2.2.4.2. Loss of Liquid Analysis*

The weight of the collagen gels exposed to self-compression on the filter paper for 20 minutes and the collagen gels subjected to plastic compression with a weight of 120 g for 5 minutes were weighed. The fluid loss between the two methods was calculated and graphically explained.

### *2.2.5. Mechanical Analysis*

The Stable Micro System TA. XT Plus Texture Analyzer was used for measuring the tensile test of collagen gels. Flexible tapes were attached to the clamps of the mini tensile grips. Thus, the samples were prevented from slipping from the clamps. Plastic compressed forms of sample C and D collagen gels were cut into a rectangular shape. Height (mm), length (mm), thickness (mm), and stress area ($mm^2$) of collagen gels were measured. Then the gels were placed between the clamps. The test speed was set to 1 mm/min. As a result of the tensile test, a stress ($\sigma$, mPa)-strain ($\varepsilon$, %) curve was obtained. Young's modulus (E) was calculated as stress ($\sigma$) /strain ($\varepsilon$) (Mori, Shimizu, and Hara 2013).

### *2.2.6. Collagen Density*

Density changes of sample C and D collagens exposed to plastic compression were calculated according to literature (Cheema et al., 2008). Wet weight of collagen gels prepared in 32 mm x 32 mm x 150 mm molds was calculated. The ratio was calculated by the dry weight of the gels exposed to 120 g plastic compression for 5 minutes (wet weight of collagen gels / dry weight of collagen gels).

### *2.2.7. AFM*

HITACHI AFM5000II was used for analysis. Analysis was started with Tap300G cantilever, q value of 425 and add value of 3.1 V. Initially, scanning was performed in the range of 50 µm x 50 µm. As the image was obtained from the sample, the dimension of the scanned area was reduced.

## 2.3. Collagen Fiber Alignment

### 2.3.1. Fiber Alignment with Electrospinning

The process was started with the electrospinning system of the INOVENSO The NS Starter Kit (Istanbul, Turkey) for forming the collagen fibers (Figure 11). Sample B (12,8 grams of bovine tendon and 0.5 M acetic acid (1/20 (w/v)) was used for electrospinning. Collagen solution was filled into a syringe with a volume of 5 ml and combined with a 0.8 mm electrically conductive stainless-steel nozzle. The voltage supply was placed between the nozzle and the $21Gx1^{1/2}$ needle tip to create a positive charge. A rectangular stainless-steel plate (21cm H x 17cm L) collector was used to create a negative charge. Stationary plate was placed in front of the voltage generator to obtain random collagen fibers. During the process, the applied voltage was changed in the range of 8-28 kW and the distance in the range of 10-20 cm. The flow rate was operated in the range of 0.05-2 ml/h.



Figure 11. INOVENSO The NS Starter Kit electrospinning system.

### 2.3.1.1. Rotating Drum Electrospinning

Then the rotating drum collector was designed for electrospinning process. It was used to create aligned collagen fibers. The rotating drum collector consists of a 23,5 cm long, 5 cm diameter stainless steel cylinder, two legs system in 20 cm H x

8,5 cm L x 4 cm W and a 7500-rpm motor (240V, 0,75A; Moonstar, China) (Figure 12). A new pulley-belt mechanism has been added to the system to reduce the rpm of the rotating drum collector motor. The following equation (2) was used to change the electrospinning rpm (Engineering ToolBox, 2010):

$$d_1 \times n_1 = d_2 \times n_2 \qquad (2)$$

Since there are 2 pulley systems, pulleys are numbered as 1 and 2. The $d_1$ and $d_2$ are driving pulley diameter (inch, mm), $n_1$ and $n_2$ are revolutions of driving pulley (rpm).

The driving pulley was 0,393 inches (in) and 7500 rpm that connected to the 240 V motor. The added new driven pulley was 4,724 inches and 623,94 rpm according to the Eq.1 (Figure 13).

The distance between the voltage generator and the collectors was changed. While optimizing the electrospinning process, two of the parameters such as distance, applied voltage and flow rate were kept constant and the other parameter was changed. The parameters (distance, flow rate and kW) used in the stationary collector was used for the rotating drum collector process.
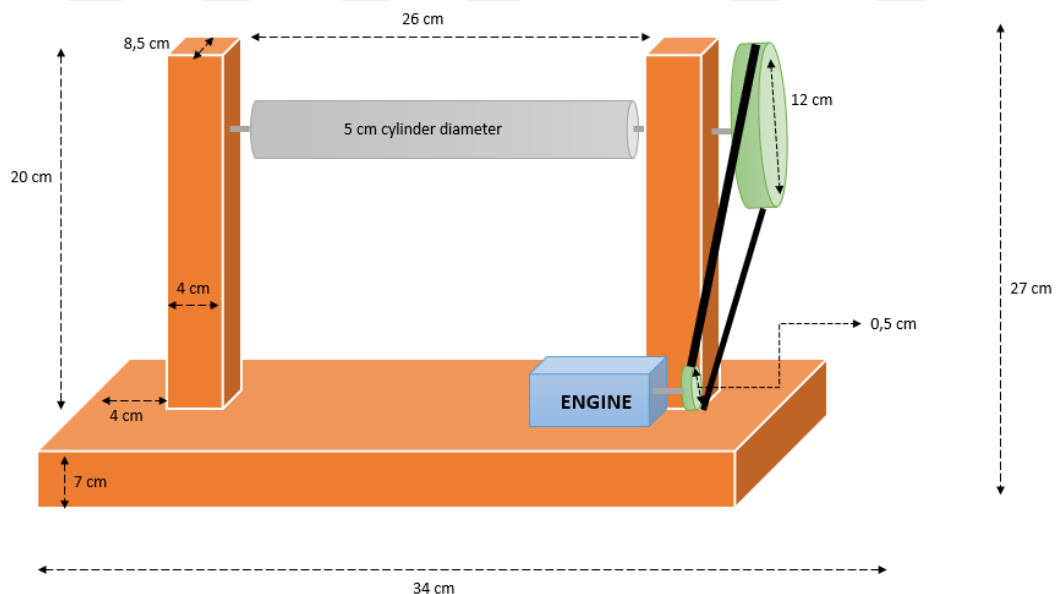


Figure 12. Hand-made rotating drum collector for electrospinning.
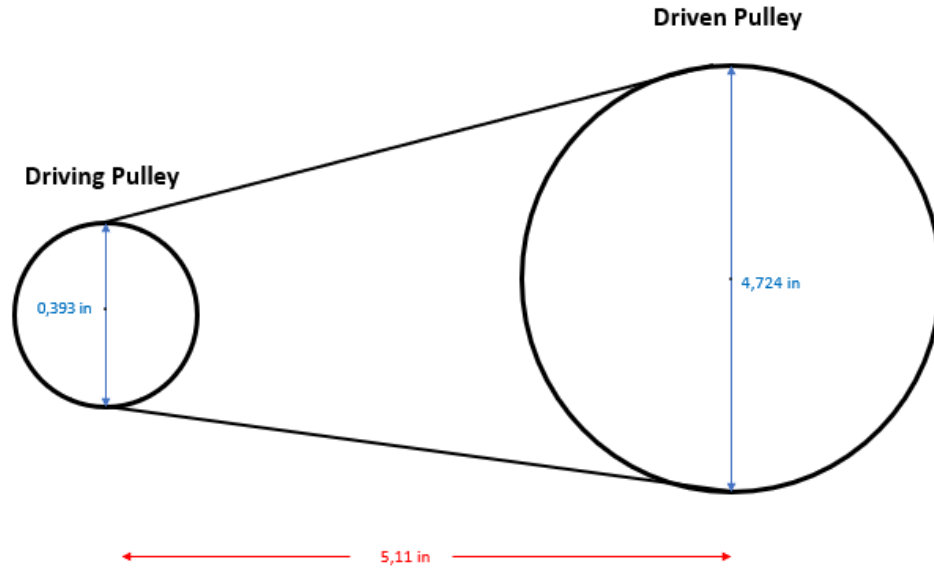
Figure 13. The new pulley-belt system for electrospinning drum collector.

### 2.3.2. Ultrasound Waves

Ultrasound waves were used as an alternative to the electrospinning method to create aligned collagen fibers. The two ends of the 15 ml centrifuge tube were cut off. A rectangular area (6 cm x 1 cm) was opened in the middle of the tube to pour the collagen gel (C) solution. Both ends of the tube were closed with parafilm. Two 20 mm piezo buzzers were placed at these two ends. Piezo buzzers were connected to the NI Elvis II+ 100 MS/s Oscilloscope (Izmir, Turkey) with electrical cables (Figure 14). A frequency was created between two piezo buzzers. The process was started with amplitude of 10 V and frequency of 2 MHz. Frequency was applied to the collagen gel for 10 minutes. Then the frequency was stopped for 1 minute. The process continued for 1 hour. The whole process was followed with NI Elvismx Instrument Launcher function generator and oscilloscope programs. The one of collagen gel taken from a 15 ml centrifuge tube was placed in a petri dish and frozen at -80 °C for lyophilization. The other gel was stored at room temperature for storage.
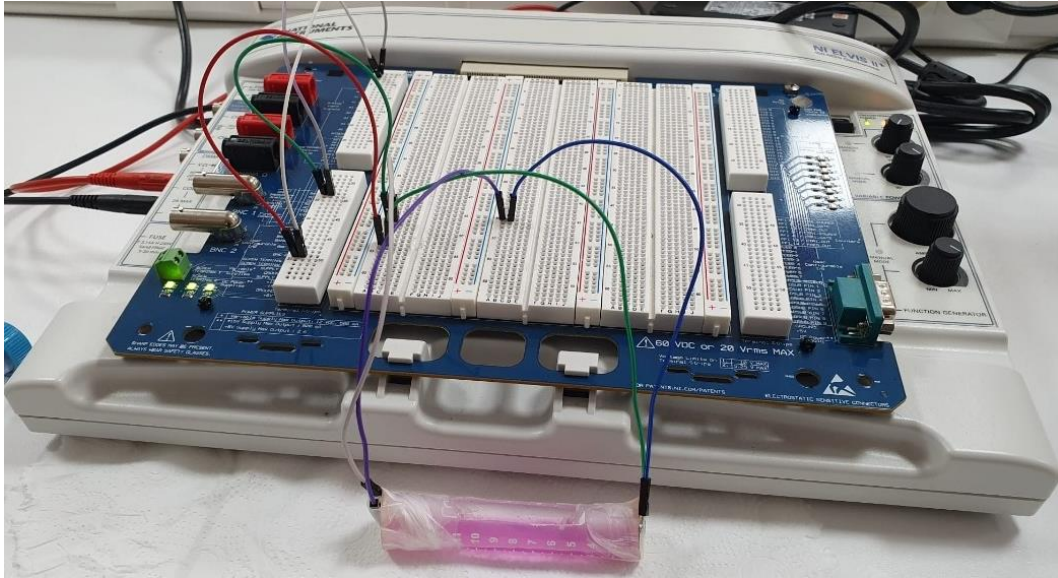
Figure 14. Ultrasound wave system for collagen fibril alignment.

### 2.3.3. Applied Force

4 ml of collagen sample (C) were placed in 60 mm x 15 mm plate. 5 M and 1 M NaOH was added until the gel form was observed. The pH of the solution was checked with pH indicator paper (IsoLab) at each step while adding NaOH. Meanwhile, the collagen solution was mixed in round circles with constant velocity by a glass stirring rod (Sigma Aldrich, diam. × 8 mm × 200 mm) for 5 minutes until 7-7,9 of pH (Figure 15). The neutralized collagen solution was left in the incubator at 37 °C for 45 minutes.
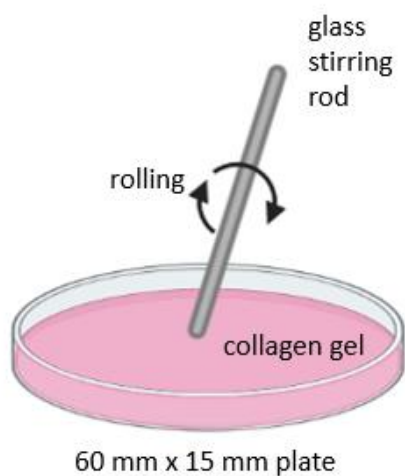


Figure 15. Collagen gel rolling procedure for collagen fiber alignment.

## 2.4. Cell Culture

### 2.4.1. Collagen Sterilization

Before starting to cell experiments, collagen sample was added to 10% chloroform (Sigma Aldrich) (according to volume of collagen) and kept at 4 °C for 24 hours (Szot et al., 2011).

### 2.4.2. Hepatocyte derived cellular carcinoma cells (Huh-7) Cell Line

Hepatocyte derived cellular carcinoma cells (*Huh-7*) were supplied by Izmir University of Economics Department of Genetics and Bioengineering (Izmir, Turkey). After removing the old medium from the cells, the cells were washed with 2x phosphate buffered saline (PBS; SEROX). Then they were incubated with trypsin-EDTA (Multicell) for 5 minutes at 37 °C in a 5% $CO_2$ incubator. They were harvested with Dulbecco's Modified Eagle Medium (DMEM; SEROX) containing high-glucose, 10% fetal bovine serum (FBS) and 1% penicillin-streptomycin (PS; Capricorn Scientific). They were centrifuged for 5 minutes at 500 G in room temperature conditions. The supernatant was discarded. Cells were dissolved in 5 ml of DMEM. Cell counts were then performed with Trypan Blue Solution (Gibco).

### 2.4.3. Huh-7 and Collagen Gels

The 1,54 ml of collagen solution (sample D), 0,193 ml 10X MEM and 0,061 ml NaOH were mixed for formation of collagen gel. 3 random collagen gel and 3 aligned collagen gel were produced. Then 360 µl *Huh-7* cell line was added to each of collagen gels in 60 mm x 15 mm plate during the gelation process. They were placed at 37 °C in a 5% $CO_2$ incubator to complete the gelation process for 30 minutes. Each collagen gel was composed of 1.500.000 cells. They were incubated for 3 days.

### 2.4.3.1. Huh-7 and Random Collagen Fibers

For observation of behavior of cells in random fibril alignment, collagen gels were produced. 360 µl *Huh-7* cell line was added to random collagen gels during the gelation process. No force was applied to the gel. After forming 3 random fibril alignment collagen gels with cells, 3 ml of DMEM was added to the gel. After 72 hours incubation, the cells were observed.

### 2.4.3.2. Huh-7 and Aligned Collagen Fibers

3 aligned collagen gels were produced for observation of behavior of cells. 360 µl *Huh-7* cell line was added to collagen solution. The alignment was done using the applied force method with the help of glass stirring rod during the gelation process for 5 minutes. The incubation process in the random collagen gel was continued in the same way for aligned collagen gels.

### 2.4.4. Optical Microscopy

At the end of 72 hours, cells were observed by optical microscopy (Euromex Oxion Inverso, Netherlands). Cells in random fiber collagen gels and aligned fiber collagen gels were compared.

### 2.4.5. PCR

Macherey-Nagel™ NucleoSpin™ RNA Mini Kit was used for RNA purification from *Huh-7* containing collagen gels. For this purpose, the Macherey-Nagel™ NucleoSpin™ RNA protocol was used. After 72 hours, the cells in the gel were taken from the incubator. 1,8 ml collagen mix and random and aligned collagen gels containing 1.500.000 cells were subjected to the protocol. Collagen gel samples were taken into a 1,5 ml centrifuge tube. Then 350 µl Buffer RA1 and 3,5 µl β-Mercaptoethanol were added to samples and vortex. After the gel was vortexed, it was placed in a NucleoSpin™ filter (violet ring) and centrifuged at 11,000 g for 1 minute. The filter was removed and 350 µl of ethanol (70%) was added to the lysate and pipetted 5 times. The mixture was transferred to the NucleoSpin™ RNA column (light blue ring) and centrifuged at 11,000 g for 30 seconds. The underlying liquid was discarded and 350 µl of Membrane Desalting Buffer (MDB) was added to the filter. It was centrifuged again at 11,000 g for 1 minute. The remaining liquid was discarded and 95 µl of DNase reaction mixture was added to the sample in the filter. The samples were incubated at room temperature for 15 minutes. Then the washing step was started. 200 µl Buffer RAW2 was added to samples with filter and centrifuged at 11,000 g for 30 seconds. The remaining liquid was discarded and 600 µl Buffer RA3 was added to NucleoSpin™ RNA Column. Then the samples were centrifuged at 11,000 g for 30 seconds. Then 250 µl Buffer RA3 was added to samples with filter and centrifuged at 11,000 g for 2 minutes.The elute RNA step

was started. 60 µl RNase-free $H_2O$ was added to samples with filter and waited 5 minutes. Then they were centrifuged at 11,000 g for 1 minute and filter was removed. The mixes containing RNA were obtained. Nanodrop device (MaestroGen) was used to determine RNA concentration and purity. 2 µl of 4 random collagen gel and 4 aligned collagen gel samples were placed in the Nanodrop device and analysis was performed.

Abm OneScript® Plus cDNA Synthesis Kit was used for cDNA synthesis from extacted RNA of collagen gels. 4 µl of 5X RT buffer, 1 µl dNTP, 1 µl primers, 1 µl OneScript® Plus RTase and 20 µl Nuclease-free $H_2O$ were mixed and it was MasterMix Solution. 8 µl RNA was taken from each sample. 12 µl of MasterMix was placed on each sample. Then cDNA samples were incubated at 50-55°C for 15 minutes. Abm BlasTaq™ 2X qPCR MasterMix Kit was used for qPCR process of collagen gels with *Huh-7*. Samples were loaded into 96 well PCR plate (0,2 ml, Nest Biotechnology) as 8x8. 5 µl of RNA of aligned collagen gels were placed in the first 4x8 wells, and 5 µl of RNA of random collagen gels were placed in the last 4x8 wells. Then 5 µl of primers were added onto the cDNA samples. Glyceraldehyde-3-Phosphate Dehydrogenase (GAPDH), Serine/Threonine Kinase 1 (AKT1), Keratin 19 (KRT19) and Krueppel-Like Factor 9 (KLF9) primers were used. Finally, 10 µl of SYBR Green™ was added to each sample. The qPCR (CFX Opus 96, Bio-Rad) process was started.

# CHAPTER 3: RESULTS

## 3.1. Collagen Extraction

### 3.1.1. SDS-Page

SDS page analysis of sample D collagen was performed using BenchMark™ Protein Ladder. Marker, 2x, x, 0,75x, 0,5x and 0,25x collagen samples were placed in the wells from left to right, respectively. The 2x contained sample D with a concentration of 3.47 M. Then, the same sample was added to the wells by dilution with 0.2 M acetic acid. According to the data in the literature using acid solubilized extraction from bovine tendon, the α1 and α2 bands of sample D are compatible. α1 and α2 bands were seen in the molecular weight range of 160 to 100 kDa. Bands lower than the molecular weight of the α chains were not clearly observed in the analysis. The results agree with standard type 1 collagen properties (Figure 16) (Ju et al., 2020).
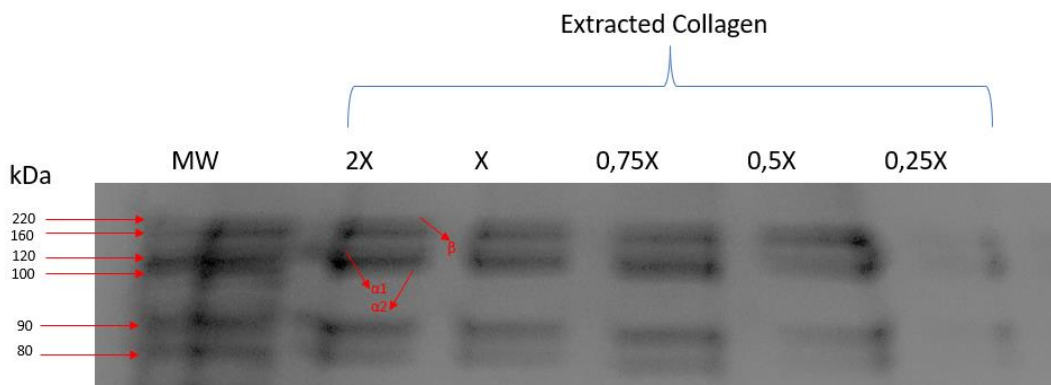


Figure 16. SDS-Page analysis of sample D collagen.

### 3.1.2. UV-Visible Spectroscopy

The commercially available collagen (BugaFibriCol Lyophilized Type I collagen from bovine flexor tendon (2 mg/ml, Eskisehir, Turkey)) was used as a reference to find the concentration of extracted collagens (Figure 17). First, the absorbance of the reference collagen dissolved as 2 mg/ml at 280 nm was measured. The serial dilution was made for concentration values and the 5 values were measured. The first collagen sample was calculated as 2 mg/ml. Then 0.35 ml of 2 mg/ml was taken and added with 0,35 ml of 0.5 M acetic acid. This solution was 1

mg/ml. For 0,75 mg/ml solution, 0,265 ml of 2 mg/ml was taken, and 0,435 ml 0,5 M acetic acid was added. For 0,5 mg/ml solution, 0,175 ml of 2 mg/ml was taken, and 0,525 ml 0,5 M acetic acid was added. Finally, 0,085 ml of 2 mg/ml was taken, and 0,613 ml 0,5 M acetic acid was added for 0,25 mg/ml. All absorbance values were measured at 280 nm wavelength. The absorbance values were measured as 0,5801, 0,3557, 0,2124, 0,1113 and 0,0786 respectively (Table 2).

Table 2. The absorbance values of different concentration at 280 nm for Buga-FibriCol.

| Concentration (mg/ml) | Absorbance at 280 nm |
|---|---|
| 2 | 0,5801 |
| 1 | 0,3557 |
| 0,75 | 0,2124 |
| 0,5 | 0,1113 |
| 0,25 | 0,0786 |

The absorbance values of the extracted collagens at different concentrations were measured (Figure 18). Absorbance values were determined 1,6153, 0,4139, 0,3183 and 1,0773 respectively for sample A, B, C and D (Table 3). Buga-FibriCol with known different concentration values and samples were compared in Excel and their concentrations were calculated by applying the formula and making graphs. Accordingly, the concentrations of the samples are 5,16 M, 1,30 M, 5,10 M, and 3,47 M respectively for sample A, B, C and D.
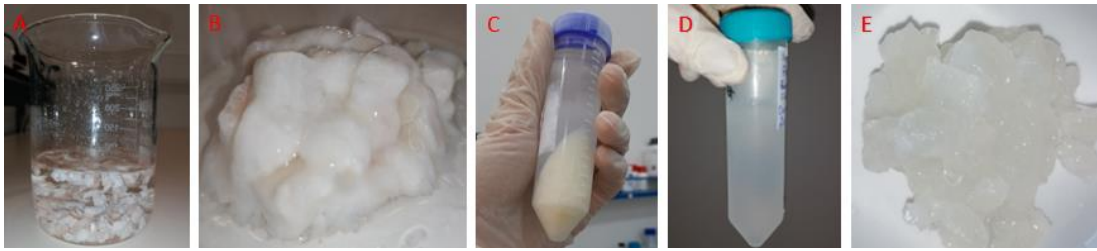
Figure 17. Acid -solubilized extracted process with bovine tendons. A) Bovine tendon pieces. B) Bovine tendon pieces after pre-treatment with EDTA. C) Centrifugation of bovine tendons and 0.2 M acetic acid solution. D) Supernatant after the centrifugation process. E) Bovine tendon pieces after acetic acid treatment.

Table 3. The concentration values of different extracted collagen.

| Sample Name | Average Absorbance at 280 nm | Concentration (M) |
|:-:|:-:|:-:|
| A | 1,583 | 5,163501 |
| B | 0,391 | 1,30054 |
| C | 1,658 | 5,10602 |
| D | 1,062 | 3,476107 |
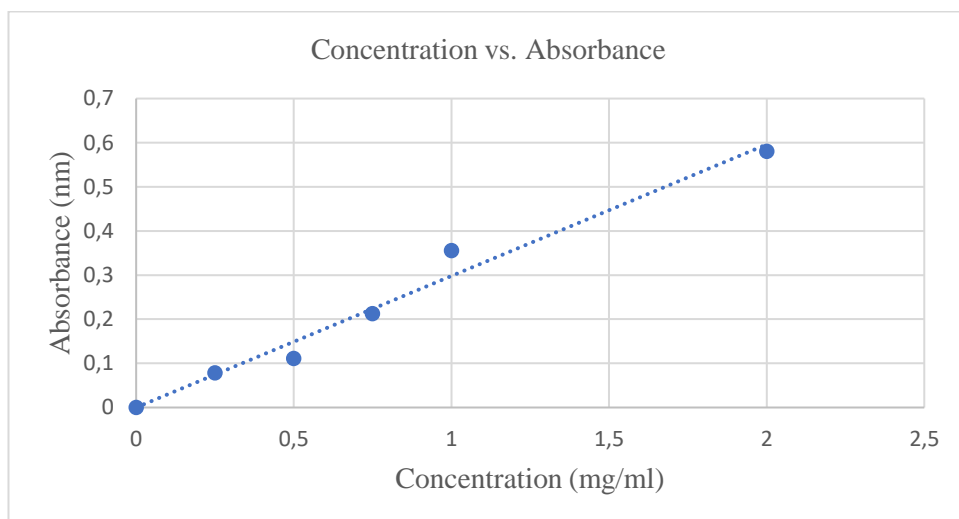


Figure 18. The graph of concentration vs. absorbance values of BugaFibriCol Lyophilized Type I collagen as a reference point to find unknown concentrations of extracted collagens.

### 3.1.3. Yield Calculation

Yield calculation was made for sample D (Figure 19) used in cell culture experiments according to the formula described in 2.1.6. The tendon and sample D collagen solution were placed in a lyophilization for 24 hours to dry. Wet weight of bovine tendon was 10,7 g and dry weight of bovine tendon was 3,549 g. Wet weight of collagen was 10,2 g and dry weight of collagen 0,361 g. According to calculations, the yield of sample D was 10,171 %.
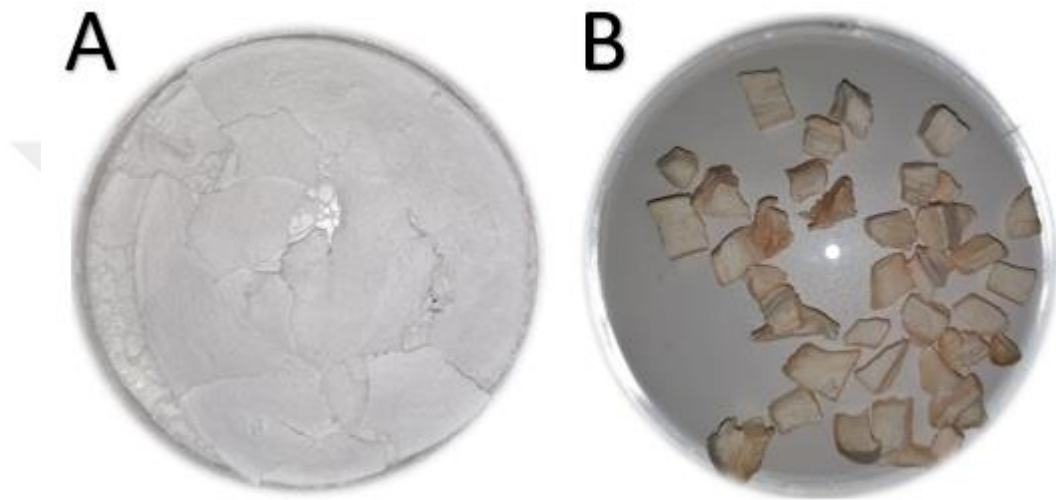


Figure 19. A) Image of lyophilized sample D collagen. B) Image of lyophilized bovine tendon of sample D.

### 3.2. Collagen Gel

### 3.2.1. Formation

Collagen gels were made from different concentration of bovine tendon solutions. The same process was applied for each sample. First of all, process was applied to sample A. When NaOH was added to sample A, clustering began to form. The precipitated collagen fiber clusters disrupted the homogeneity of the gel. The sample B collagen gel was homogeneous and easily removed from the mold (Figure 20). The gel process was applied to samples C and D that were dialyzed and only filtered. Sample C and D was suitably converted to gel form, like sample B.

Figure 20. Collagen gel from sample B.

### 3.2.2. Plastic-Compression of Collagen Gel

After compression, sample B, C and sample D (Figure 21 and Figure 22) had a homogeneous form. They were easily removed from the nylon meshes and kept at room temperature for a few days. The liquid in the gels evaporated at room temperature, but the gel forms did not deteriorate. The weight difference of the plastic compression applied sample C gel and D were measured with 120 g for 5 minutes. Each measurement was repeated 3 times. The average initial weight of the sample C gel was 3,412 g and the gel was weighed as 0,135 g after 5 minutes on average (Figure 23). The average initial weight of the sample D gel was 3,516 g and the gel was weighed as 0,246 g after 5 minutes on average.
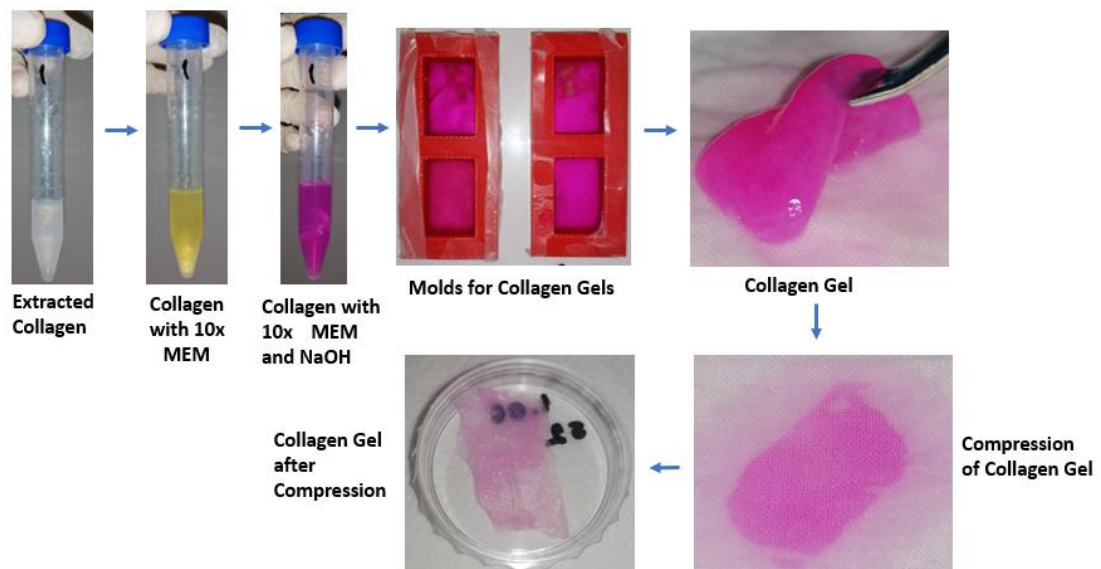


Figure 21. Process of collagen gel production and plastic compression.

Figure 22. Plastic compression of sample D collagen gel.
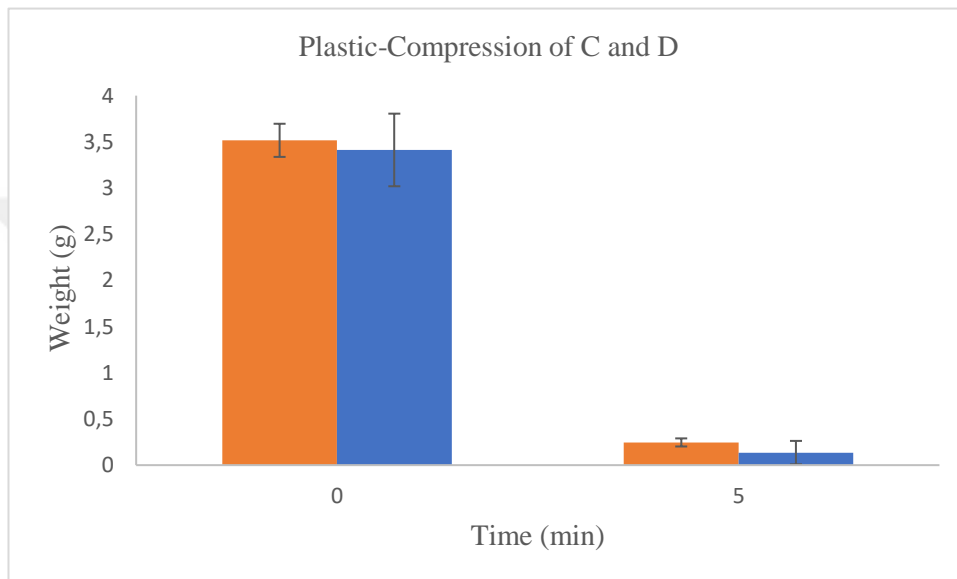


Figure 23. Weights of sample C and D collagen gel before and after plastic compression process (blue line = sample C, orange line = sample D).

### 3.2.3. Self-Compression of Collagen Gel

Sample C and D gels were made in a mold (32,12 mm x 32,12 mm x 150 mm) for observing of self-compression behavior (Figure 24). After 45 minutes of gel processing, the weight of the collagen gels was measured. Each measurement was repeated 3 times and average values are given. The measurement was done at 2-min intervals. Sample C and D were allowed to loss of liquid for 20 min. The average weights were given in the Table 4 and the loss of liquid graph of the gel was drawn (Figure 25). Between 0 and 2 minutes, liquid loss was the highest with 2,181 g and 2,600 g for C and D, respectively. The second highest liquid loss was seen between 2 and 4 minutes. They were 0,371 g and 0,335 grams for C and D, respectively. After the 4th minute, the fluid loss gradually decreased. There was a fluid loss of 2,974 g

between the first measurement and the last measurement for C. According to measurement, total liquid loss of D was 3,318 g.
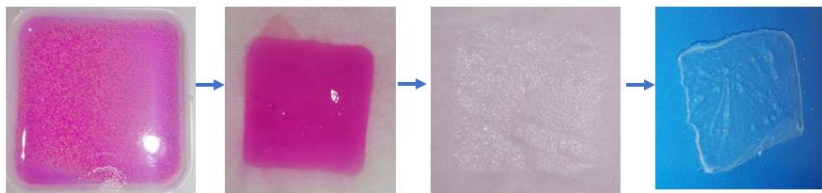


Figure 24. Self-compression process of collagen gel for 20 min.

Table 4. Measurement of liquid loss for sample C and D after self-compression method (average values).

| Sample name | 0 min | 2 min | 4 min | 6 min | 8 min | 10 min | 12 min | 14 min | 16 min | 18 min | 20 min |
|---|---|---|---|---|---|---|---|---|---|---|---|
| C (g) | 3,6 | 1,45 | 1,08 | 0,94 | 0,88 | 0,83 | 0,78 | 0,75 | 0,73 | 0,70 | 0,66 |
| D (g) | 3,7 | 1,13 | 0,79 | 0,67 | 0,59 | 0,53 | 0,50 | 0,47 | 0,44 | 0,43 | 0,41 |
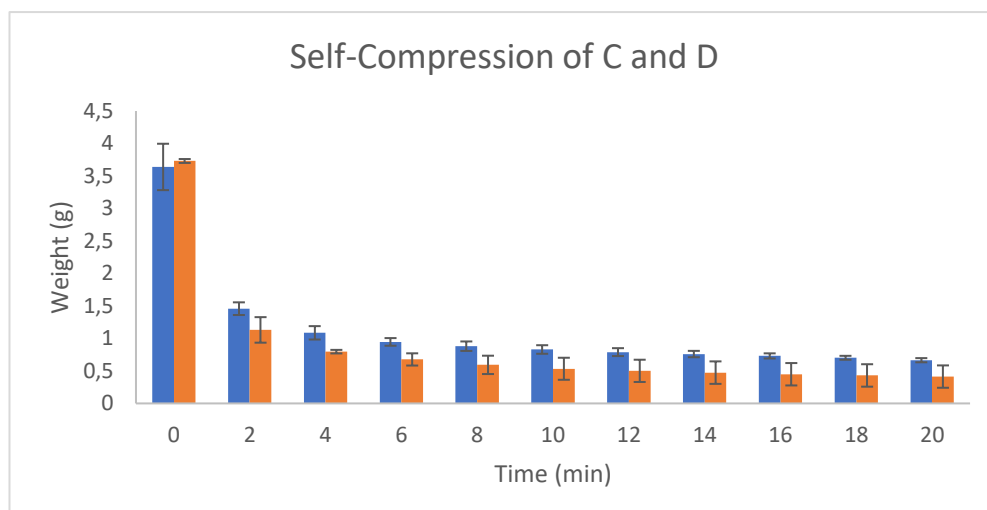


Figure 25. Weights of sample C and D collagen gel before and after self-compression process (blue line = sample C, orange line = sample D).

### 3.3. Physical Characterization

### 3.3.1. Length, Height, and Thickness of Collagen Gels

The thickness of compressed gels was measured by micrometer (Table 5). 3 plastic compressed samples C and 3 plastic compressed sample D were measured. The average thicknesses of 3 sample C were 0,041 mm, 0,056 mm and 0,056 mm. The average thicknesses of 3 plastic compressed sample D were 0,025 mm, 0,028 mm and 0,022 mm. The height and length values of sample C are 22 mm, 19 mm, 21 mm and 19 mm, 14 mm, 18 mm, respectively. And also, the height and length values of sample D are 26 mm, 26 mm, 25 mm and 21 mm, 20 mm, 21 mm, respectively. The height and length measurements of sample C and D were compared in Figure 26.

Table 5. Thickness, height, and length measurement of plastic compressed collagen gels.

| Sample Name | | Avarage Thickness (mm) | Height (mm) | Length (mm) |
|---|---|---|---|---|
| Sample C | 1. | 0,041 | 22 | 19 |
| | 2. | 0,056 | 19 | 14 |
| | 3. | 0,056 | 21 | 18 |
| Sample D | 1. | 0,025 | 26 | 21 |
| | 2. | 0,028 | 26 | 20 |
| | 3. | 0,022 | 25 | 21 |
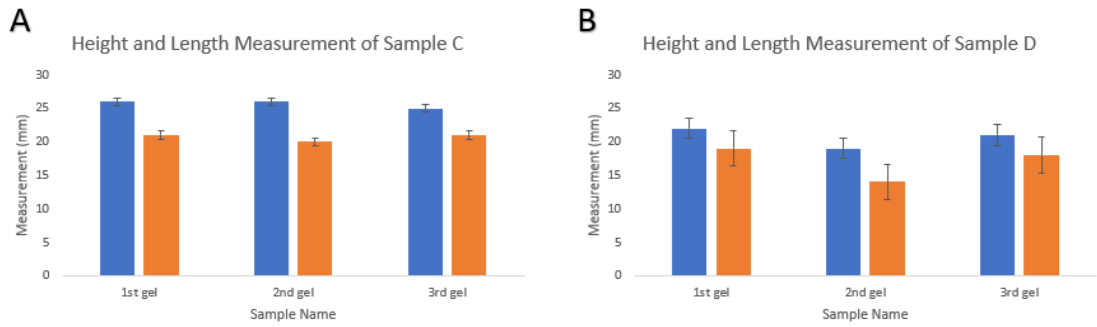
Figure 26. A) Height and length measurement of sample C collagen gels. B) Height and length measurement of sample D collagen gels (blue line=height values, orange line=length values).

## 3.4. Mechanical Analysis

Tensile strength test was performed on plastic compressed sample C and D gels (Figure 27 and 28) whose dimensions were measured. Stress value of sample C (stress area= 0,847 mm$^2$, length=17 mm) was 27,319 mPa, and strain value was 58,764 %. Stress of 3 sample D (stress area= 0,611 mm$^2$, length=17 mm) was 3,553 mPa and strain of sample D was 29,352 %. Young's Modulus of sample C and D were 0,464 N/m$^2$ and 0,121 N/m$^2$, respectively.
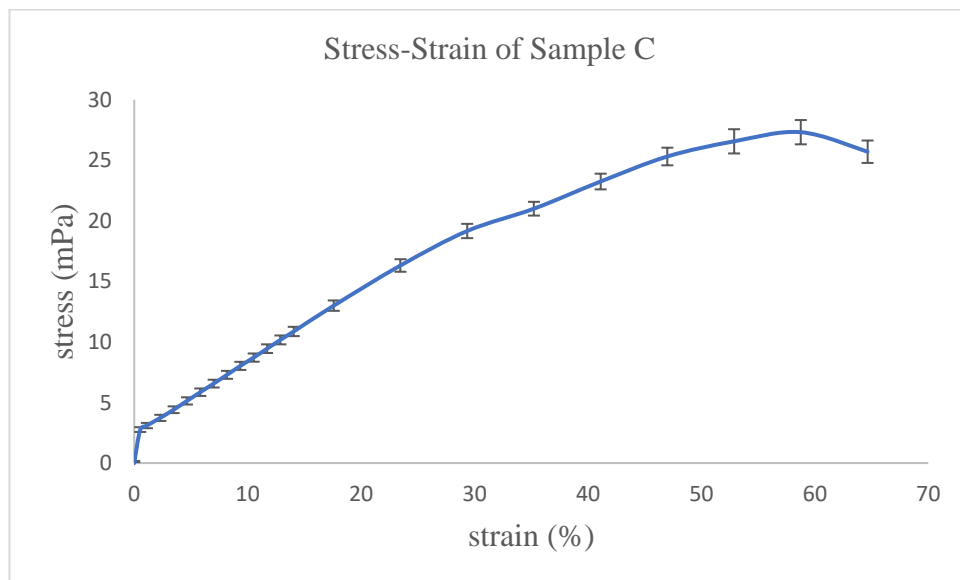


Figure 27. Stress-strain curve of sample C collagen gel (stress =27,319 mPa, strain= 58,764%).
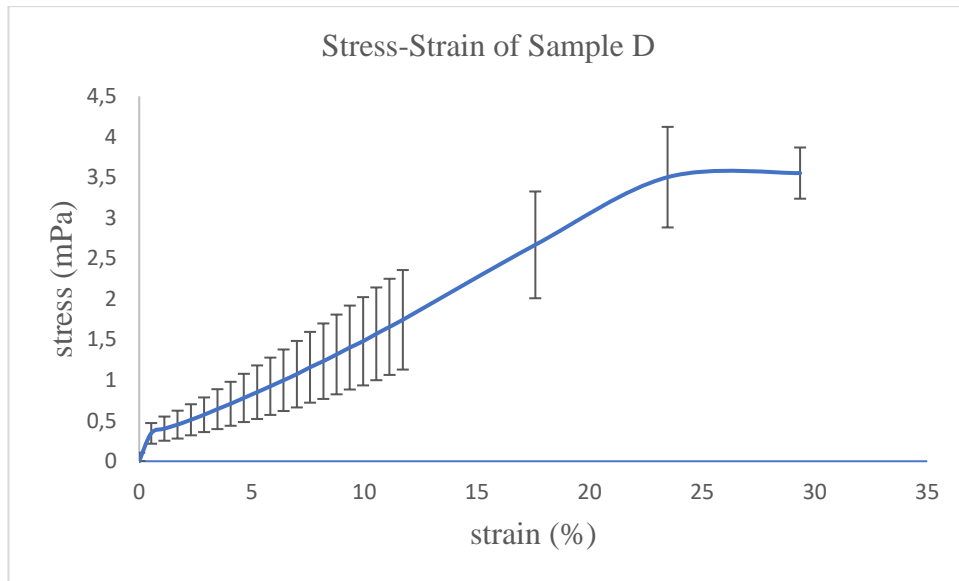
Figure 28. Stress-strain curve of sample D collagen gel (stress=3,553 mPa, strain=29,352%).

### 3.5. Collagen Density

Collagen density ratios of collagen gels were examined, which were applied compression with 120 g weight for 5 minutes to investigate effect of plastic compression method. 4 ml of collagen solution was used in 5 ml of total collagen gel solution. Before plastic compression sample C was 3,161 grams. The dry weight of sample C was measured as 0,261 grams after the plastic compression method. When the same process was applied for sample D, the wet weight was 3,541 g and the dry weight was 0,250. The initial collagen concentration was accepted as 0,51% for sample C. The volume for sample C decreased by 91.75% after plastic compression. Accordingly, the collagen density ratio increased by 23,4% after plastic compression applied the initial collagen gel volume of 5 ml. The initial collagen concentration was accepted as 0,347% for sample D. The volume for sample D decreased by 92,94% after plastic compression. The collagen density ratio increased by 12,9%.

The change in collagen density in 5 ml collagen gel solution exposed to self-compression for 20 minutes was calculated. The initial weight of sample C was 3,639 g and after self-compression weight of sample C was 0,665 g. Sample D was 3,731 g before the self-compression. The final weight of sample D was 0,413 g. Collagen density of sample C increased by 16,69% after self-compression and collagen density change of sample D increased by 12,34%.

### 3.6. Collagen Fiber Alignment

### 3.6.1. Electrospinning

Rectangular plate collector was used to generate random collagen fibrils. First of all, the flow rate was kept constant. The voltage value and the distance were changed. The flow rate was determined as 0.5 ml/h and the voltage was changed in the range of 8-25 kV. At the same time the distance was changed in the range of 10-20 cm. Taylor cone formation at the tip of the needle was used to prove fiber formation. Taylor cone was not observed throughout the process and the collagen solution reached the plate as a droplet. The experiment continued with the same parameters by increasing the flow rate to 1 ml/h. However, the experiment was stopped because Taylor cone formation was not observed. Then the flow rate was reduced to 0.05 ml/h and then a Taylor cone was formed at 0.05 ml/h, 10 cm, and 28-30 kV. With this result, it was aimed to decrease the kV value and to increase the distance between the plate and the needle. As a result, random collagen fibers were formed at 0.05 ml/h, 12-14 cm and 18-22 kV for 3 hours. Aluminum foil was removed from the stationary collector and a visible collagen deposition was confirmed. The sample was examined under a light microscope (Nikon Eclipse LV150N) to get more precise results (Figure 29A). Successful production of random electrospun collagen fibrils was observed.

0.05 ml/h, 10-14 cm and 18-22 kV values were used for aligned collagen fibers by electrospinning rotating drum collector. The electrospinning process was carried out for 3 hours at the 623,94 rpm. Taylor's cone was observed at the tip of the needle. After the process was finished, the aluminum foil was examined. Unlike the stationary collector, collagen deposition was not observed on the aluminum foil. Aluminum foil was examined under a light microscope for a more effective examination. As a result, very few and broken collagen fibers were observed on the drum collector (Figure 29B).

The random and aligned collagen fibrils produced by the electrospinning method were examined by AFM (Figure 30). Firstly, the collagen fibers produced by electrospinning were imaged. It has been proven that the random fibers are produced successfully with the stationary collector electrospinning method. Random fibers

with diameters between 20-60 nm had a length of 500 nm approximately. The number of aligned fibers to be produced with rotating drum collector electrospinning was very low amount and short. Aligned electrospun fibers were negligible compared to random electrospun fibers.
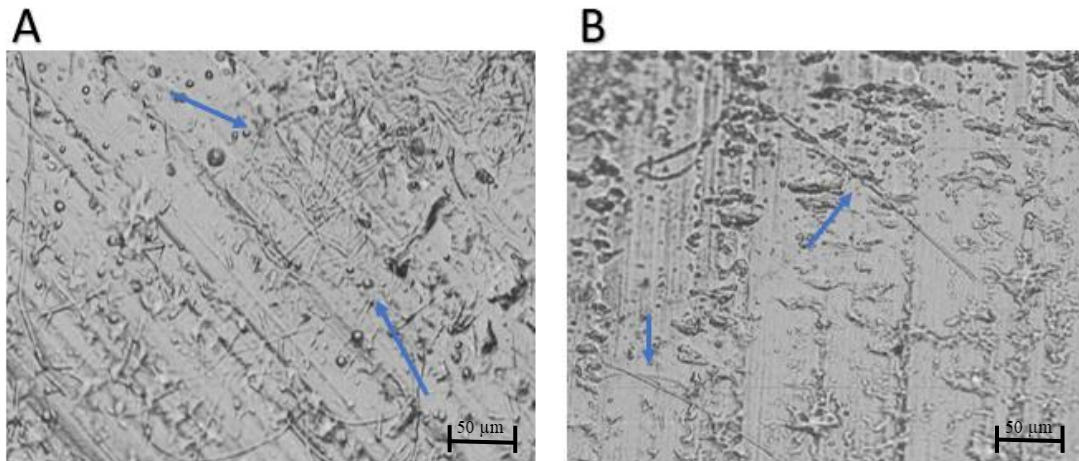


Figure 29. A) Microscopic analysis of random electrospun collagen fibrils on aluminum foil (50 µm). B) Microscopic analysis of aligned electrospun collagen fibrils aluminum foil (50 µm).
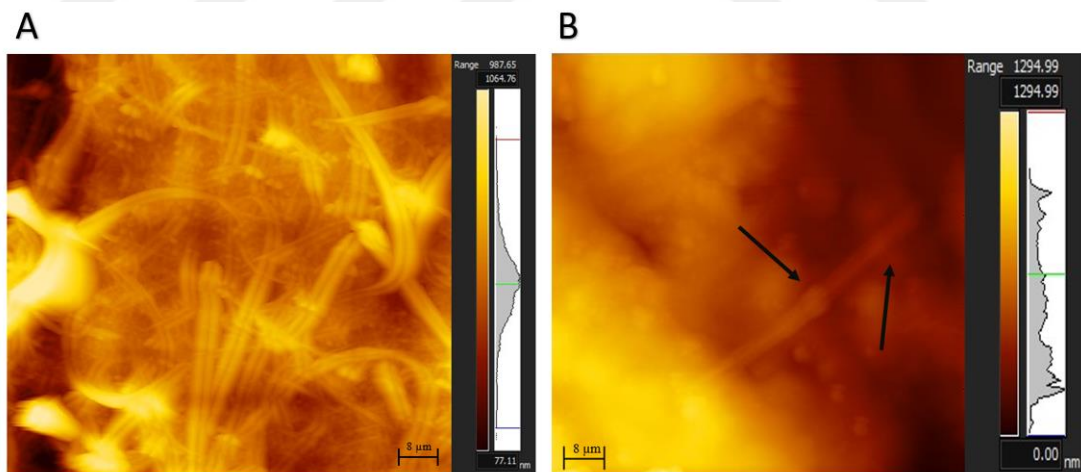


Figure 30. A) AFM analysis of random electrospun collagen fibers (8 µm), B) AFM analysis of aligned (8 µm) electrospun collagen fibers.

### 3.6.2. Ultrasound Waves

Collagen fibril alignment using ultrasound waves was examined by AFM analysis. 2 MHz and 10V frequency was applied to the collagen gel for 1 hour. As a result of the AFM analysis, it was proved that the collagen fibrils were aligned with this method (Figure 31).
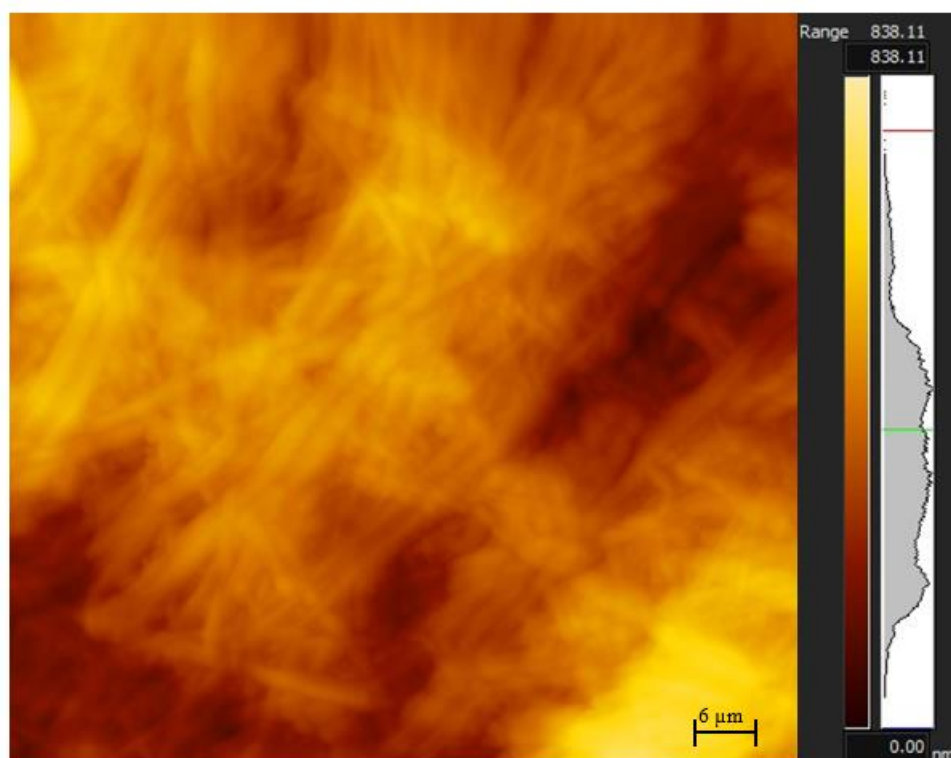


Figure 31. AFM analysis of collagen fibril alignment with ultrasound waves (6 µm).

### 3.6.3. Applied Force

The aligned collagen gel by force and random collagen gel (Figure 33) were compared. The aligned collagen gel produced by the force method was imaged (Figure 32). Here it is proved that there is an order between the fibers. The aligned collagen gel fibers were approximately 60 nm in diameter and 150 nm in length. A dense fiber structure was seen stacked on top of each other.
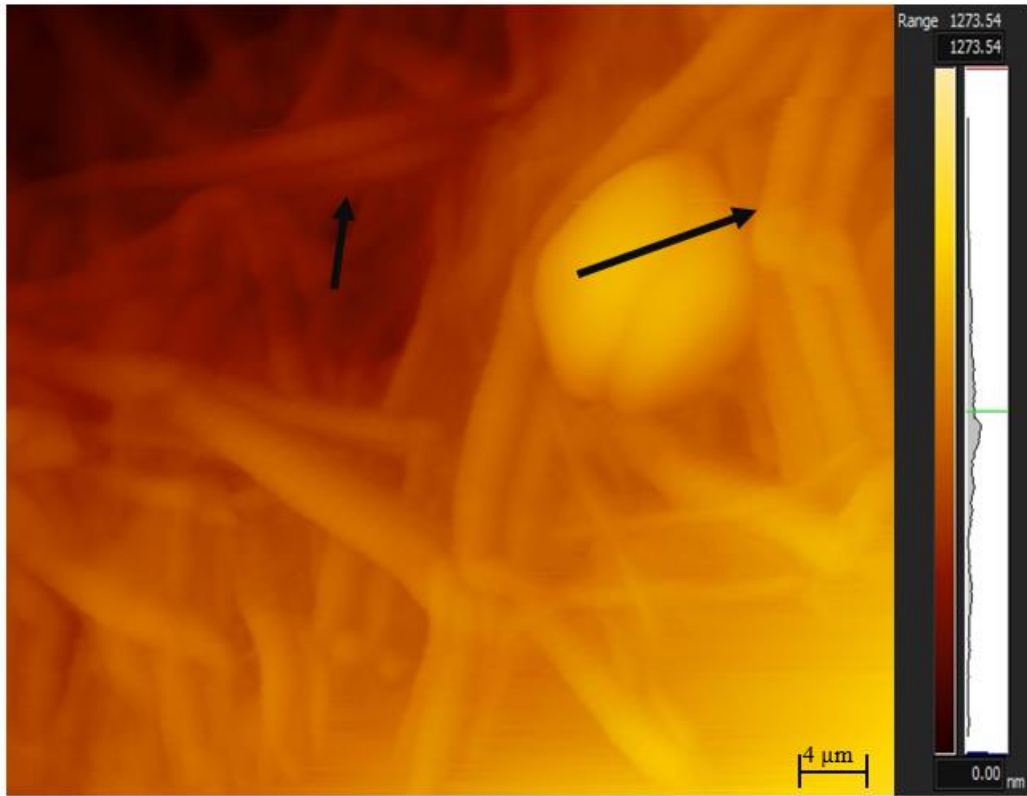
Figure 32. AFM analysis of aligned collagen gel by force (4 µm).
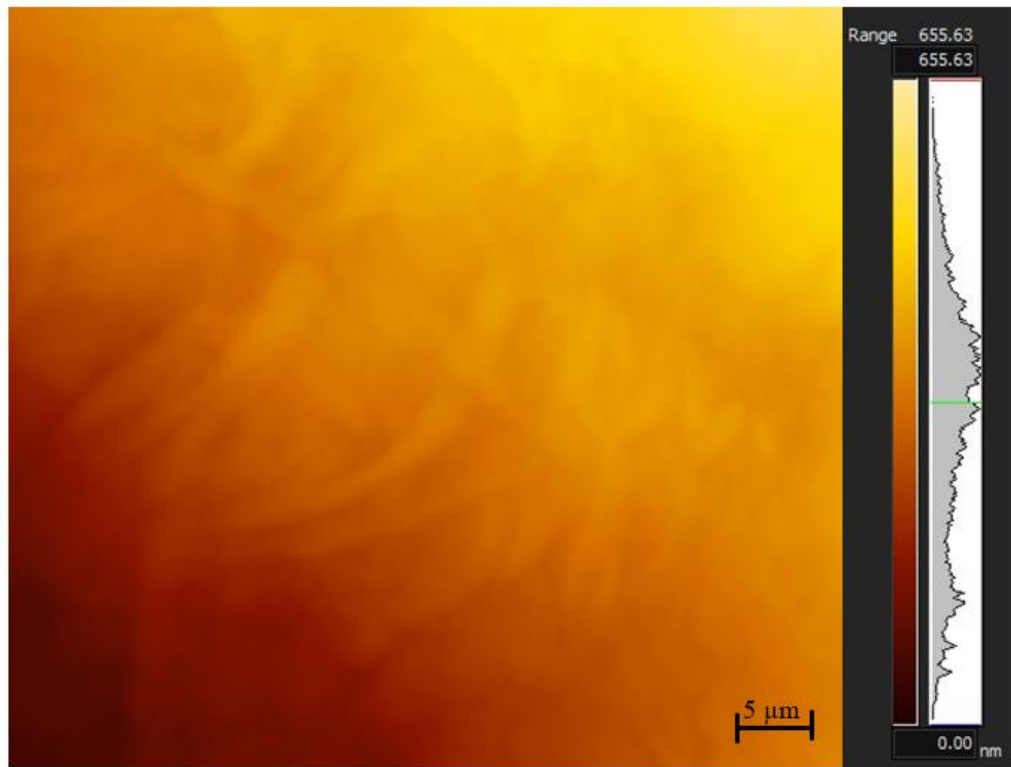


Figure 33. AFM analysis of random collagen gel (5 µm).

### 3.7. Cell Culture

Image of random and aligned collagen gels containing 1,500,000 of *Huh-7* at the end of 72 hours were taken under an optical microscope (Figure 34). Cells appeared embedded in the gels and arranged in layers within the gels.
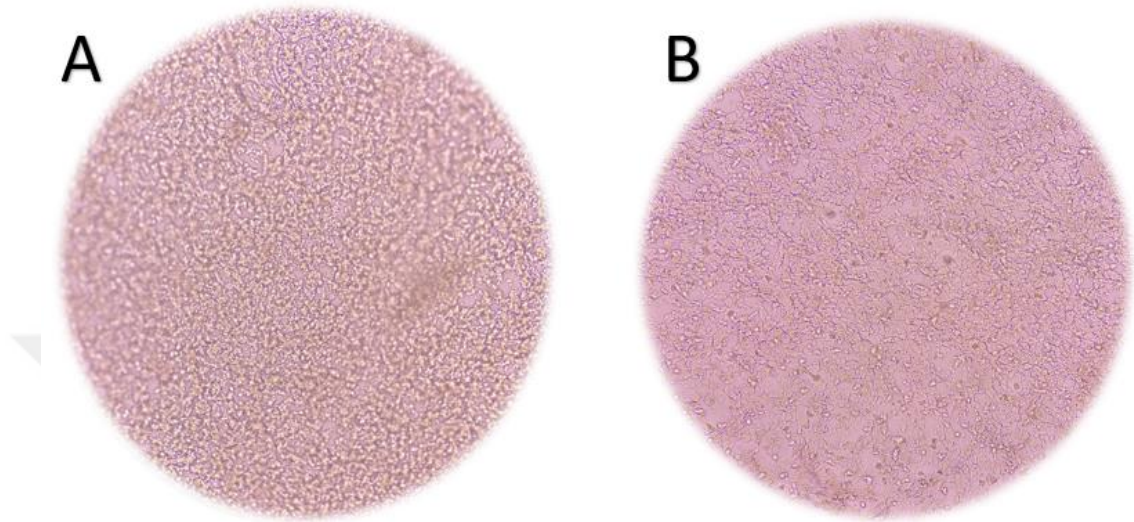


Figure 34. A) Random collagen gels with *Huh-7*. B) Aligned collagen gel with *Huh-7*.

Also, *Huh-7* cells were seeded into collagen fibrils arranged as random and aligned, and the expression of Akt1, Krt19, Klf9, Hnf1a and Hnf4a genes was examined with qPCR after 3 days of incubation. Beta actin was used as housekeeping gene and analysis results were plotted accordingly (Figure 35). The Hnf4a gene controls proliferation and invasion in cancer cells (Lv, Zhou and Tang, 2021). For aligned collagen gel samples, there was upregulation trend in expression Hnf1a and Hnf4a. Also, Hnf1a supports hepatocyte behavior in cancer stem cells by providing cell homeostasis (Wang et al., 2019). Krt19 is a hepatic stem/progenitor cells marker. It is known that 28% of hepatocellular carcinoma cells express Krt19. This rate is far below the expression of Krt19 in hepatocyte cells. On the other hand, in the light of studies, it has been proven that the Krt19 gene supports the development of fibrotic tumors in hepatocellular carcinoma cells (Rhee et al., 2018). According to the results of the study, trend upregulation was seen in the Krt19 expression. The Klf9 gene acts as a tumor suppressor gene and has been shown to be downregulated for hepatocellular carcinoma in the literature (Sun et al., 2014). When the hepatocellular carcinoma Klf9 gene expression level in aligned and random

collagen gels was examined, no statistically significant difference was found. The main element regulating the PI3K molecular pathway is the Akt1 gene. Cells interacting with the collagen molecule around portal tracts activate the PI3K molecular pathway through Akt1 gene and integrin signals. Thus, tumor formation of cells accelerates. In addition, the Akt1 gene contributes to the survival characteristics of the cells. Therefore, this gene increases the prognosis of the disease in patients with liver fibrosis (Mroweh et al., 2021). No statistically significant results were found for Akt1 expression of *Huh-7* cells in aligned collagen fibrils.
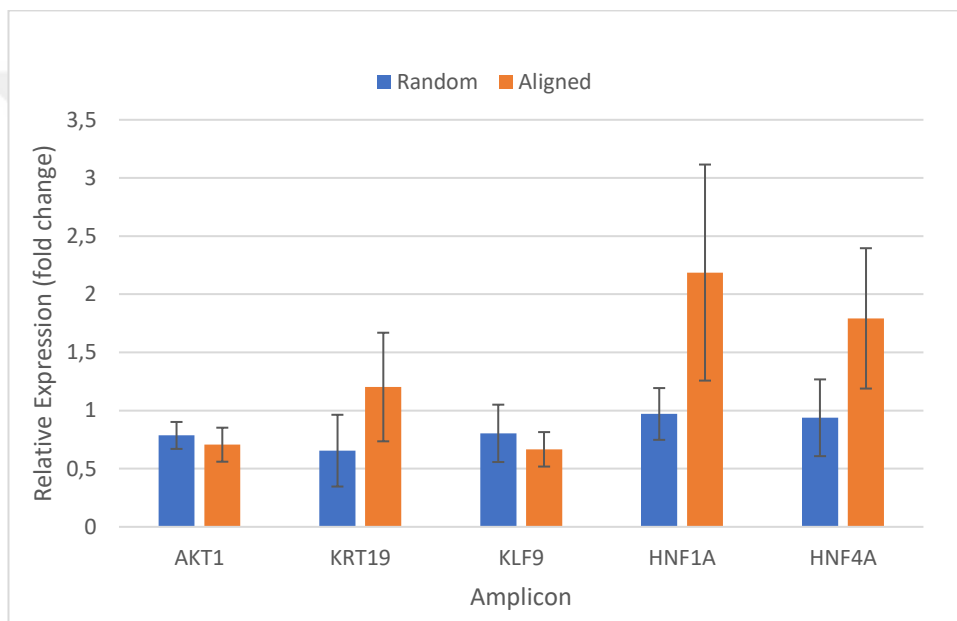


Figure 35. Relative expressions of Akt1, Krt19, Klf9, Hnf1a and Hnf4a were calculated using the Beta actin. Blue lines represent random collagen gel and orange lines represent aligned collagen gel. Error bars represent SEM values.

# CHAPTER 4: DISCUSSION

In this study, the effect of collagen fibril alignment on hepatocellular carcinoma cells by modeling liver fibrosis. Collagen plays a major role in liver structure and liver fibrosis disease. As explained in the introduction section, the collagen fibril arrangement changes in liver fibrosis. Therefore, it was desired to mimic different collagen fibril arrangements for investigation behavior of liver cancer cells.

For this purpose, it was aimed to extract collagen, which is the first stage of the experiment. Many different sources are used for collagen extraction such as marine animals, bovine tendons, and rat tails. Rat tails and bovine tendons are generally used in the production of collagen-based hydrogels for use in biomedical applications (Blidi et al., 2021). Researchers have proven that collagen hydrogel increases cell viability and differentiation in fibroblast cells (Tabatabaei, Moharamzadeh, and Tayebi, 2020). They also said that collagen extracted from bovine tendon enhances cell viability, differentiation, and wound healing (Cui et al., 2020). In this study, bovine tendon was used for collagen extraction due to its easy accessibility, cheapness and frequently use in the literature.

It is important to apply pretreatment steps before collagen extraction. The physical aim here is to remove unwanted substances from the surface of the material and to increase the surface area of the source to be extracted. And also, it aims to break intermolecular covalent bonds (Matinong et al., 2022). In this study, Tris-NaCl and EDTA were used to prevent protein degradation in the pre-treatment stage. The difference between the two is that the Tris-NaCl has a pH buffering function (Sepmag, 2022).

Three different methods are generally used for collagen extraction such as neutral salt extraction, acid solubilized extraction and enzymatic extraction. The researchers said that collagen yield of acid solubilized extraction is higher than other methods, and the chemicals are used with simpler process (Blidi et al., 2021). Thanks to acetic acid, collagen molecules show an electrostatic repulsive force. In this way, molecules are easily separated, cross-links are broken. And also, the acid solubilized extraction method has been used in study because it is a convenient method for

extracting fibrils in collagen. Extraction was continued at 4 °C to prevent protein degradation (Matinong et al., 2022). In the extraction of sample A and B, the ratio of 0.5 M acetic acid was 1/20 (w/v). While 12,8 g of sample B showed gelation, 8,8 grams of sample A did not. Among the reasons for this is the possibility that sample A is exposed to a high amount of acetic acid, which has a low bovine tendon mass, and all covalent and non-covalent bonds between collagen molecules may be broken. In addition, the purchase of bovine tendons from different suppliers and the different age and breed of the animal may have affected the collagen extraction (Matinong et al., 2022). With this extraction method, properties such as viscosity and concentration of collagen can be easily affected. The short pretreatment time in sample A may also have affected the gelation process by slowing down extraction. Sample C and D had the same mass and same ratio of acetic acid (1/20 (w/v)). Both samples were found to be successful in the gelation process. The concentration values of the two samples (C and D) were different from each other and the bovine tendon samples were different from each other. As mentioned before, the living conditions and age of the animal from which the tendon is taken greatly affect the collagen extraction. Dialysis method with 0.5 M acetic acid used as purification method for 48 hours. The gelation of treated with post treatment method and untreated was compared for sample C. The whole process was applied the same in two samples. No difference in gelation was observed.

Collagen dissolved in acetic acid was neutralized with NaOH for SDS-Page analysis. Because acetic acid disrupted the gel structure used in the analysis. Collagen solution was diluted in order to see the bands clearly. In this way, the existence of bands of collagen at different concentrations was proven.

NaOH was used to neutralize the acidic collagen solution throughout the gelation process. In this way, the collagen both showed gel properties and the acidic environment was removed, which was fatal for the cells. Some fibril fragments were observed to precipitate as NaOH was added during the gelling procedure. Salts containing strong anions and cations can cause precipitation without affecting the pH of the collagen solution (Matinong et al., 2022). During acetic acid extraction, it was observed that the centrifuged solution had two phases. While the supernatant portion contained monomeric collagen, re-exposure of collapsed tendon fragments to acid

treatment led to the observation of the polymeric portion of the collagen. The supernatant containing both monomeric collagen and polymeric collagen caused fibril collapse while neutralizing the gel. The collapsed fibrils can be subjected to acid treatment and salting-out processes again. In this way, the polymeric collagen portion of the collagen solution can be converted into monomeric collagen by a separate process.

Temperature and pH are the factors affecting gelation during the collagen gelation process. It is very suitable for showing collagen gel behavior at 7-7,4 pH and 37 °C. If the pH value is at alkaline or acidic values, the process will fail. Under these conditions, mechanical analysis of gel is quite difficult such as tensile strength. Therefore, compression methods are used to improve conditions. A reduction of 91,75% and 92,94% in dimension was observed in plastic compression-applied collagen gels. Thanks to the fluid loss after compression, the amount of collagen density also increased by 23,4% and 12,9% in a standard gel. Differences in the amount of collagen density are related to the concentration of collagen solutions. After compression, collagen solutions with higher concentration have lower fluid loss while collagen density change is greater such as sample C. Therefore, the thickness of the high concentration plastic compressed sample is greater.

After being compressed, standard 4 ml collagen gels were subjected to tensile strength analysis. It was investigated how long 2 biopolymers of different densities could withstand the applied force. The compress was applied to improve the mechanical properties by removing the liquid from the gels. A standard tendon stress strain curve is given in the Figure 36. When a force is applied to the tendon, primarily the fibrils in its content begin to change their structure up to a 2% strain. The region where this behavior is seen is called the toe region. In the linear region of the graph, the fibers become flat and after a certain force, the fibrils begin to rupture (Sensini and Cristofolini, 2018). The tensile strength of the native tendon is considerably higher than samples C and D. Because while other tissues and structures support the tendon, it was also large in the stress area where the force was applied. Sample C with a collagen concentration of 5,10 M and sample D with a concentration of 3,47 M were analyzed. As a result of tensile strength analysis

performed at 1 mm/sec and ASTM standards, it was seen that high density sample C was more resistant to force than sample D.
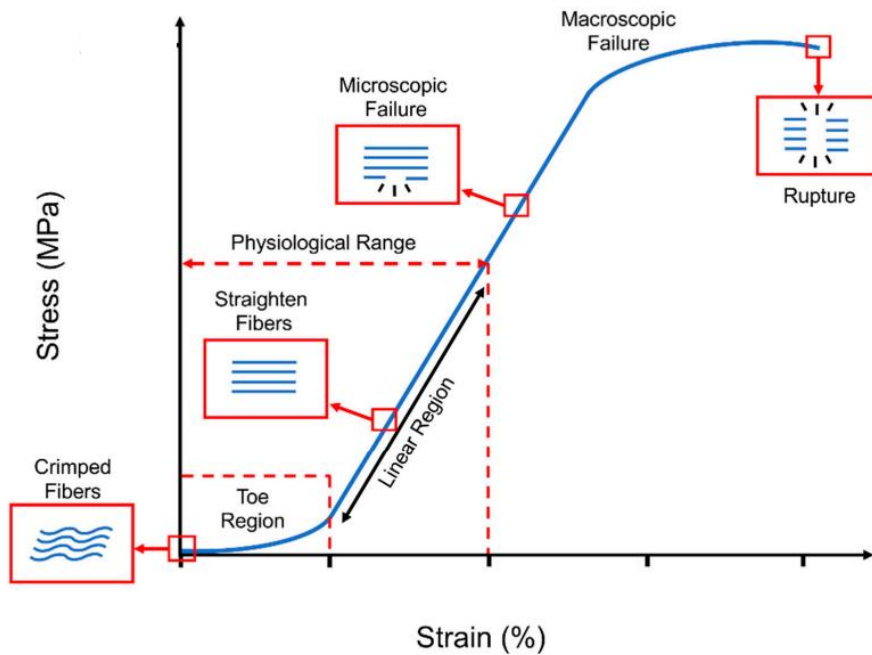


Figure 36. Stress-strain curve of tendon (Source: Sensini and Cristofolini, 2018).

Collagen fibril alignment was aimed to be able to model after collagen extraction. So, three different alignment methods were used such as electrospinning, ultrasound waves and force applied. Collagen solution with 1.37 M concentration was used for electrospinning. In order to produce random collagen fibrils, collector type stationary was chosen as a flat plate. Electrospinning process continued at 0.05 ml/h, 12-14 cm and 18-22 kV conditions for 1, 2 and 3 hours. At the end of 3 hours, the collagen fiber density accumulated in the collector was examined under the microscope and AFM. It was thought that the fibril density was suitable for modeling. Then, the rotating drum collector was designed for the regular alignment of the collagen fibrils. The same sample used for random alignment was used for this process. The 5 cm diameter steel pipe and 7500 rpm 240 V motor were connected to the system as collector. The electrospinning process continued at 0.05 ml/h, 12-14 cm and 18-22 kV conditions for 3 hours. At the end of the process, when examined under the microscope, it was observed that there was short, broken and few collagen fibrils. Since the rpm of collector was very high throughout the process, it was aimed to reduce this speed. For this purpose, a new pulley-belt system was created.

Diameter of new system was approximately 12 times larger than the original pulley system diameter. The goal here was to reduce the collector rpm by 12 times. With the 2 pulley-belt system, the rpm of the engine would slow down, and the collector's sample collection would slow down. In this way, more collagen fibrils would appear on the collector. With this design, rpm of the rotating drum collector was 623,94. The fibril alignment electrospinning process was examined under the microscope, which continued 3,4 and 5 hours. It was observed that the collagen fibrils on the collector were short and broken. At the same time, it was concluded that the number of fibrils was insufficient to make a tissue model. The reason why the electrospinning device did not have a closed system caused it to be affected by the temperature, humidity and the dust in the environment. Under these unfavorable conditions, the experimental parameters were variable. Therefore, the electrospinning process for collagen fibril alignment could not be standardized. In addition, the collagen fibrils on the aluminum surface were difficult to sterilize for cell experiments in the collector. Because the fibril density on the collector was uncertain and it was difficult to determine the ratio of the chemical to be used for sterilization. Performing cell experiments with these samples would have negative results, as aluminum foil may be toxic to cells.

For collagen fibril alignment, aligning using ultrasound waves was attempted after the electrospinning process. Collagen gels applied at 2 MHz and 10V frequency with the help of an oscilloscope were examined under AFM. Ultrasound waves delivered to the gel at 10-minute intervals for 1 hour caused collagen fibril alignment. Using this method for cell experiments was difficult in terms of sterilization and time. It was not known what kind of cell behavior and vitality would be encountered as a result of giving frequency to the cells for 1 hour. In order to use this method, it was decided that more optimization was required.

For cell experiments, the applied mechanical force method was used to align the collagen fibrils. With this method, some gene expressions of *Huh-7* cells in the aligned collagen gel were examined. Along with the qPCR results, there was an upregulation trend of Krt19, Hnf1a and Hnf4a genes although not statistically significant was seen in liver cancer cells. The upregulation trend of Hnf4a seen in aligned collagen gels suggests that hepatocellular carcinoma cells may proliferate by

acting more aggressively in this fibrillar arrangement. The low levels of Hnf1a seen in the random collagen gel suggest that the hepatocyte behavior of cancer stem cells can be inhibited. It has been proven by previous studies that aligned collagen fibrils are more common around portal tracts than random fibrils. Considering this information, Akt1 gene expression in the aligned collagen gel was expected to be upregulated. In this study, a statistically significant conclusion could not be reached about the relationship between the survival abilities of hepatocellular carcinoma cells and the collagen fibrillar structure. With the observation of upregulation trend of Krt19 in aligned collagen fibrils, it was thought that *Huh-7* cells would support aggressive tumor development with the help of arranged fibrils. At the same time low levels of Klf9 expression in aligned collagen gels may enhance tumor presence. Research is needed to interpret this gene expression.

In this study, it was previously presented that some gene expressions were examined in order to examine the behavior of hepatocellular carcinoma cells. The reason why there was no statistically significant result at the end of the study may be due to collagen gels. Collagen gels arranged as aligned and random fibrils may not be heterogeneously spread on the petri dish. Therefore, the number of cells in the gel may not be equal in all parts of the gel. This may have distorted the statistical meaning of aligned and random gels. The mechanical force method can be replaced and optimized with other alignment methods when aligning collagen fibrils. Thus, the dispersion of hepatocellular carcinoma cells in the gel may be heterogeneous. Because of the stochastic effects of collagen gels, error bars may be excessive in gene expression. This may have made it difficult for us to obtain statistically significant results. Although not statistically significant, Hnf1a, Hnf4a and Krt19 upregulation trend results raise the possibility of aggressive proliferation of hepatocellular carcinoma cells in aligned collagen gels.

# CHAPTER 5: CONCLUSION

Collagen is a frequently studied biopolymer due to its abundance in the human body and its wide-ranging mechanism of action. The arrangement of collagen fibrils has an importance ranging from connective tissues to diseases. The fibril arrangement of collagen changes with external factors such as internal factors and alcohol use, pathogens which is abundant in the liver structure. This change causes diseases such as fibrosis and cirrhosis in the liver. Cells interacting with collagen molecules through molecular signals can induce cancer-causing molecular pathways and cause liver cancer formation. In this study, the fibril structure of collagen gels with mechanical force was changed and hepatocellular carcinoma cells were seeded into the changing fibril structure. The aim here is to examine the effect of fibril structure on hepatocellular carcinoma cells and to see how collagen contributes to disease progression. As a result of the experiments, it was observed that hepatocellular carcinoma cells affected some gene expressions in aligned collagen gels. The upregulation trend although not statistically significant in Hnf1a and Hnf4a genes, it is thought that aligned collagen gels contribute to the proliferation and differentiation of hepatocellular carcinoma cells. In the future, changes in the behavior of cells can be studied using all fibril alignment methods. Thus, in future studies, it can be understood more clearly how liver fibrosis contributes to cancer formation.

# REFERENCES

Anwanwan, D., Singh, S. K., Singh, S., Saikam, V. and Singh, R. (2020) *Challenges in liver cancer and possible treatment approaches,* Biochimica et Biophysica Acta-Reviews on Cancer [Online]. Available at: https://pubmed.ncbi.nlm.nih.gov/31682895/ (Accessed: 1 January 2021).

Alison, M. R. (2005) *Liver stem cells: Implications for hepatocarcinogenesis,* Stem Cell Reviews, 1(3), pp. 253–260.

Arias, I.M., Alter, H.J., Boyer, J.L., Cohen, D.E., Shafritz, D.A., Thorgeirsson, S.S. and Wolkoff, A.W. (2020) *The Liver: Biology and Pathobiology,* 5th edition. UK: John Wiley & Sons Ltd.

Bataller, R. and Brenner, D. A. (2005) *Science in medicine Liver fibrosis,* The Journal of Clinical Investigation, 115(2), pp. 209–218.

Bell, C. C., Hendriks, D. F. G., Moro, S. M. L., Ellis, E., Walsh, J., Renblom, A., Fredriksson Puigvert, L., Dankers, A. C. A., Jacobs, F., Snoeys, J., Sison-Young, R. L., Jenkins, R. E., Nordling, Å., Mkrtchian, S., Park, B. K., Kitteringham, N. R., Goldring, C. E. P., Lauschke, V. M. and Ingelman-Sundberg, M. (2016) *Characterization of primary human hepatocyte spheroids as a model system for drug-induced liver injury, liver function and disease,* Scientific Reports [Online]. Available at: https://www.nature.com/articles/srep25187 (Accessed: 4 May 2016).

Blidi, O. El, Omari, N. El, Balahbib, A., Ghchime, R., Menyiy, N. El, Ibrahimi, A., Kaddour, K. Ben, Bouyahya, A., Chokairi, O. and Barkiyou, M. (2021) *Extraction methods, characterization and biomedical applications of collagen: A review,* Biointerface Research in Applied Chemistry, 11(5), pp. 13587–13613.

Brashear, S. E., Wohlgemuth, R. P., Gonzalez, G. and Smith, L. R. (2021) *Passive stiffness of fibrotic skeletal muscle in mdx mice relates to collagen architecture,* Journal of Physiology, 599(3), pp. 943–962.

Bray, F., Ferlay, J., Soerjomataram, I., Siegel, R. L., Torre, L. A. and Jemal, A. (2018) *Global cancer statistics 2018: GLOBOCAN estimates of incidence and mortality worldwide for 36 cancers in 185 countries,* A Cancer Journal for Clinicians, 68(6), pp. 394–424.

Briesewitz, R., Epstein, M. R. and Marcantonio, E. E. (1993) *Expression of native and truncated forms of the human integrin α1 subunit,* Journal of Biological Chemistry, 268(4), pp. 2989–2996.

Brown, R. A. (2013) *In the beginning there were soft collagen-cell gels: Towards better 3D connective tissue models?,* In Experimental Cell Research, 319(16), pp. 2460–2469.

Buttafoco, L., Kolkman, N. G., Engbers-Buijtenhuijs, P., Poot, A. A., Dijkstra, P. J., Vermes, I. and Feijen, J. (2006) *Electrospinning of collagen and elastin for tissue engineering applications,* Biomaterials, 27(5), pp. 724–734.

Carloni, V., Mazzocca, A., Pantaleo, P., Cordella, C., Laffi, G. and Gentilini, P. (2001) *The integrin, α6β1, is necessary for the matrix-dependent activation of FAK and MAP kinase and the migration of human hepatocarcinoma cells,* Hepatology, 34(1), pp. 42–49.

Chen, G., Xia, B., Fu, Q., Huang, X., Wang, F., Chen, Z. and Lv, Y. (2019) *Matrix mechanics as regulatory factors and therapeutic targets in hepatic fibrosis,* International Journal of Biological Sciences, 15(12), pp. 2509–2521.

Chen, W., Rock, J. B., Yearsley, M. M., Ferrell, L. D. and Frankel, W. L. (2014) *Different collagen types show distinct rates of increase from early to late stages of hepatitis C-related liver fibrosis,* Human Pathology, 45(1), pp. 160–165.

Cheema, U., R. A. Brown, B. Alp and A. J. MacRobert, (2008) *Spatially defined oxygen gradients and vascular endothelial growth factor expression in an engineered 3D cell model*. Cellular and Molecular Life Science, 65, pp. 177–186.

Chiang, J. Y. L. and Ferrell, J. M. (2018) *Bile acid metabolism in liver pathobiology,* Gene Expression, 18(2), pp. 71–87.

Cui, B., Zhang, C., Gan, B., Liu, W., Liang, J., Fan, Z., Wen, Y., Yang, Y., Peng, X. and Zhou, Y. (2020) *Collagen-tussah silk fibroin hybrid scaffolds loaded with bone mesenchymal stem cells promote skin wound repair in rats,* Materials Science and Engineering C [Online]. Available at: https://pubmed.ncbi.nlm.nih.gov/32228999/ (Accessed: 28 December 2019).

Delaine-smith, R. M., Green, N. H., Matcher, S. J., Macneil, S. and Reilly, G. C. (2014) *Monitoring Fibrous Scaffold Guidance of Three- Dimensional Collagen Organisation Using Minimally- Invasive Second Harmonic Generation*, PLoS ONE [Online]. Available at: https://journals.plos.org/plosone/article?id=10.1371/journal.pone.0089761 (Accessed: 28 February 2014).

Diehl, A. M. (2002) *LIVER REGENERATION*, Frontiers: Bioscience, 7, pp. 301–314.

Elango, J., Hou, C., Bao, B., Wang, S., Maté Sánchez de Val, J. E. and Wenhui, W. (2022) *The Molecular Interaction of Collagen with Cell Receptors for Biological Function,* Polymers [Online]. Available at: https://www.ncbi.nlm.nih.gov/pmc/articles/PMC8912536/ (Accessed: 23 February 2022).

Eguchi, Y., Ogiue-Ikeda, M. and Ueno, S. (2003) *Control of orientation of rat Schwann cells using an 8-T static magnetic field*, Neuroscience Letters, 351(2), pp. 130–132.

Engelholm, L. H., List, K., Netzel-Arnett, S., Cukierman, E., Mitola, D. J., Aaronson, H., Kjøller, L., Larsen, J. K., Yamada, K. M., Strickland, D. K., Holmbeck, K., Danø, K., Birkedal-Hansen, H., Behrendt, N. and Bugge, T. H. (2003) *uPARAP/Endo180 is essential for cellular uptake of collagen and promotes fibroblast collagen adhesion.* Journal of Cell Biology, 160(7), pp. 1009–1015.

Ferraro, V., Gaillard-Martinie, B., Sayd, T., Chambon, C., Anton, M. and Santé-Lhoutellier, V. (2017) *Collagen type I from bovine bone. Effect of animal age, bone anatomy and drying methodology on extraction yield, self-assembly, thermal behaviour and electrokinetic potential,* International Journal of Biological Macromolecules, 97, pp. 55–66.

Gadiya, M. and Chakraborty, G. (2018) *Signaling by discoidin domain receptor 1 in cancer metastasis,* In Cell Adhesion and Migration, 12(4), pp. 315–323.

Gailhouste, L., Grand, Y. Le, Odin, C., Guyader, D., Turlin, B., Ezan, F., Désille, Y., Guilbert, T., Bessard, A., Frémin, C., Theret, N. and Baffet, G. (2010) *Fibrillar*

collagen scoring by second harmonic microscopy: A new tool in the assessment of liver fibrosis, Journal of Hepatology, 52(3), pp. 398–406.

Girton, T. S., Barocas, V. H. and Tranquillo, R. T. (2002) Confined compression of a tissue-equivalent: Collagen fibril and cell alignment in response to anisotropic strain, Journal of Biomechanical Engineering, 124(5), pp. 568–575.

Guo, C. and Kaufman, L. J. (2007) Flow and magnetic field induced collagen alignment, Biomaterials, 28(6), pp. 1105–1114.

Henriksen, J. H. and Møoller, S. (2004) Hypertension and liver disease, Current Hypertension Reports, 6(6), pp. 453–461.

Hocking, D. C., Sottile, J. and Langenbach, K. J. (2000) Stimulation of integrin-mediated cell contractility by fibronectin, Journal of Biological Chemistry, 275(14), pp. 10673–10682.

Holmes, D. F., Gilpin, C. J., Baldock, C., Ziese, U., Koster, A. J. and Kadler, K. E. (2001) Corneal collagen fibril structure in three dimensions: Structural insights into fibril assembly, mechanical properties, and tissue organization, Proceedings of the National Academy of Sciences of the United States of America, 98(13), pp. 7307–7312.

Iredale, J. P., Thompson, A. and Henderson, N. C. (2013) Extracellular matrix degradation in liver fibrosis: Biochemistry and regulation, Biochimica et Biophysica Acta - Molecular Basis of Disease, 1832(7), pp. 876–883.

Kim, J. and Kim, C. S. (2018) Harnessing nanotopography of PCL/collagen nanocomposite membrane and changes in cell morphology coordinated with wound healing activity, Materials Science and Engineering C, 91, pp. 824–837.

Ju, H., Liu, X., Zhang, G., Liu, D. and Yang, Y. (2020) Comparison of the Structural Characteristics of Native Collagen Fibrils Derived from Bovine Tendons Using Two Different Methods: Modified Acid-Solubilized and Pepsin-Aided Extraction, Materials [Online]. Available at: https://www.researchgate.net/publication/338551871_Comparison_of_the_Structural _Characteristics_of_Native_Collagen_Fibrils_Derived_from_Bovine_Tendons_Usin

g_Two_Different_Methods_Modified_Acid-Solubilized_and_Pepsin-Aided_Extraction (Accessed: 8 January 2020).

DeMali, K. A., Wennerberg, K. and Burridge, K. (2003) *Integrin signaling to the actin cytoskeleton*, Current Opinion in Cell Biology, 15(5), pp. 572–582.

Keirouz, A., Chung, M., Kwon, J., Fortunato, G. and Radacsi, N. (2020) *2D and 3D electrospinning technologies for the fabrication of nanofibrous scaffolds for skin tissue engineering: A review,* Wiley Interdisciplinary Reviews: Nanomedicine and Nanobiotechnology, 12(4), pp. 1626–1658.

Labrador, J. P., Azcoitia, V., Tuckermann, J., Lin, C., Olaso, E., Mañes, S., Brückner, K., Goergen, J.-L., Lemke, G., Yancopoulos, G., Angel, P., Martínez-A, C. and Klein, R. (2001) *The collagen receptor DDR2 regulates proliferation and its elimination leads to dwarfism*, EMBO Reports, 2(5), pp. 446-452.

Levis, H. J., Brown, R. A. and Daniels, J. T. (2010) *Plastic compressed collagen as a biomimetic substrate for human limbal epithelial cell culture*, Biomaterials, 31(30), pp. 7726–7737.

Li, D., Mu, C., Cai, S., and Lin, W. (2009) *Ultrasonic irradiation in the enzymatic extraction of collagen*, Ultrasonics Sonochemistry, 16(5), pp. 605–609.

Lin, J., Pan, S., Zheng, W. and Huang, Z. (2013) *Polarization-resolved second-harmonic generation imaging for liver fibrosis assessment without labeling*, Applied Physics Letters, 103(17), pp. 173701-173706.

Liu, C., Zhu, C., Li, J., Zhou, P., Chen, M., Yang, H. and Li, B. (2015) *The effect of the fibre orientation of electrospun scaffolds on the matrix production of rabbit annulus fibrosus-derived stem cells*, Bone Research [Online]. Available at: https://www.nature.com/articles/boneres201512 (Accessed: 9 June 2015).

LiverTox: Clinical and Research Information on Drug-Induced Liver Injury (2012) *Regorafenib*, Bethesda (MD): National Institute of Diabetes and Digestive and Kidney Diseases [Online]. Available at: https://www.ncbi.nlm.nih.gov/books/ (Accessed: 6 June 2018).

Lv, H., Li, L., Sun, M., Zhang, Y., Chen, L., Rong, Y. and Li, Y. (2015) *Mechanism of regulation of stem cell differentiation by matrix stiffness*, Stem Cell Research and Therapy [Online]. Available at: https://pubmed.ncbi.nlm.nih.gov/26012510/ (Accessed: 27 May 2017).

Lv, D. D., Zhou, L. Y. and Tang, H. (2021) *Hepatocyte nuclear factor 4α and cancer-related cell signaling pathways: a promising insight into cancer treatment*, Experimental and Molecular Medicine, 53(1), pp. 8–18.

Matinong, A. M. E., Chisti, Y., Pickering, K. L. and Haverkamp, R. G. (2022) *Collagen Extraction from Animal Skin*, Biology, 11(6), pp. 905–920.

Matthews, J. A., Wnek, G. E., Simpson, D. G. and Bowlin, G. L. (2002) *Electrospinning of collagen nanofibers*, Biomacromolecules, 3(2), pp. 232-238.

Meyaard, L. (2008) *The inhibitory collagen receptor LAIR-1 (CD305)*, Journal of Leukocyte Biology, 83(4), pp. 799–803.

McCoy, M. G., Wei, J. M., Choi, S., Goerger, J. P., Zipfel, W. and Fischbach, C. (2018) *Collagen Fiber Orientation Regulates 3D Vascular Network Formation and Alignment*, ACS Biomaterials Science and Engineering, 4(8), pp. 2967–2976.

Mori, H., Shimizu, K. and Hara, M. (2013) *Dynamic viscoelastic properties of collagen gels with high mechanical strength*, Materials Science and Engineering C, 33(6), pp. 3230–3236.

Mroweh, M., Roth, G., Decaens, T., Marche, P. N., Lerat, H. and Jílková, Z. M. (2021) *Targeting AKT in hepatocellular carcinoma and its tumor microenvironment*, International Journal of Molecular Sciences, 22(4), pp. 1794–1808.

Nikolaou, K., Sarris, M. and Talianidis, I. (2013) *Molecular pathways: The complex roles of inflammation pathways in the development and treatment of liver cancer*, Clinical Cancer Research, 19(11), pp. 2810–2816.

Ohtani, O. (1992) *The Maceration Technique in Scanning Electron Microscopy of Collagen Fiber Frameworks: Its Application in the Study of Human Livers*, Archives of Histology and Cytology, 55, pp. 225–232.

Okuyama, K., Xu, X., Iguchi, M. and Noguch, K. (2005) *Revision of Collagen Molecular Structure*, Biopolymers, 84(2), pp. 181-191.

Ozaki, I., Hamajima, H., Matsuhashi, S. and Mizuta, T. (2011) *Regulation of TGF-β1-induced pro-apoptotic signaling by growth factor receptors and extracellular matrix receptor integrins in the liver,* Frontiers in Physiology [Online]. Available at: https://www.ncbi.nlm.nih.gov/pmc/articles/PMC3199809/ (Accessed: 24 October 2011).

Porter, R. A., Brown, R. A., Occleston, N. L., Peng, P. and Khaw, T. (1998) *Ultrastructural changes during contraction of collagen lattices by ocular fibroblasts*, Wound Repair and Regeneration, 6(2), pp. 157-166.

Provenzano, P. P., Inman, D. R., Eliceiri, K. W., Knittel, J. G., Yan, L., Rueden, C. T., White, J. G. and Keely, P. J. (2008) *Collagen density promotes mammary tumor initiation and progression*, BMC Medicine [Online]. Available at: https://bmcmedicine.biomedcentral.com/articles/10.1186/1741-7015-6-11 (Accessed: 28 April 2008).

Rhee, H., Kim, H. Y., Choi, J. H., Woo, H. G., Yoo, J. E., Nahm, J. H., Choi, J. S. and Park, Y. N. (2018) *Keratin 19 expression in hepatocellular carcinoma is regulated by fibroblast-derived HGF via a MET-ERK1/2-AP1 and SP1 Axis*, Cancer Research, 78(7), pp. 1619–1631.

Riching, K. M., Cox, B. L., Salick, M. R., Pehlke, C., Riching, A. S., Ponik, S. M., Bass, B. R., Crone, W. C., Jiang, Y., Weaver, A. M., Eliceiri, K. W. and Keely, P. J. (2014) *3D Collagen Alignment Limits Protrusions to Enhance Breast Cancer Cell Persistence,* Biophysical Journal, 107(11), pp. 2546–2558.

Rieder, F., Brenmoehl, J., Leeb, S., Schölmerich, J. and Rogler, G. (2007) *Wound healing and fibrosis in intestinal disease*. Gut, 56(1), pp. 130–139.

Ringehan M., McKeating J.A. and Protzer U. (2017) *Viral hepatitis and liver cancer*. Philosophical Transactions B. [Online]. Available at: https://www.ncbi.nlm.nih.gov/pmc/articles/PMC5597741/ (Accessed: 11 September 2017).

Rouède, D., Schaub, E., Bellanger, J.-J., Ezan, F. and Tiaho, F. (2020) *Wavy nature of collagen fibrils deduced from the dispersion of their second-order nonlinear optical anisotropy parameters ρ*, Optics Express, 28(4), pp. 4845-4858.

Sacchi, M., Bansal, R. and Rouwkema, J. (2020) *Bioengineered 3D Models to Recapitulate Tissue Fibrosis*, Trends in Biotechnology, 38(6), pp. 623-636.

Sell, S. and Leffert, H. L. (2008) *Liver cancer stem cells*, Journal of Clinical Oncology, 26(17), pp. 2800–2805.

Shrivastava, A., Radziejewski, C., Campbell, E., Kovac, L., McGlynn, M., Ryan, T.E., Davis, S., Goldfarb, M.P., Glass, D.J., Lemke, G. and Yancopoulos, G. (1997) An Orphan Receptor Tyrosine Kinase Family Whose Members Serve as Nonintegrin Collagen Receptors. Molecular Cell, 1(1), pp. 25–34.

Sieghart, W., Hucke, F., Pinter, M., Graziadei, I., Vogel, W., Müller, C., Heinzl, H., Trauner, M. and Peck-Radosavljevic, M. (2013) *The ART of decision making: Retreatment with transarterial chemoembolization in patients with hepatocellular carcinoma*, Hepatology, 57(6), pp. 2261–2273.

Sensini, A. and Cristofolini, L. (2018) *Biofabrication of electrospun scaffolds for the regeneration of tendons and ligaments*, Materials [Online]. Available at: https://www.ncbi.nlm.nih.gov/pmc/articles/PMC6213815/ (Accessed: 12 October 2018).

Simpson, D. G., Jha, B. S., Ayres, C. E., Bowman, J. R., Telemeco, T. A., Sell, S. A. and Bowlin, G. L. (2011) *Electrospun collagen: A tissue engineering scaffold with unique functional properties in a wide variety of applications*, Journal of Nanomaterials [Online]. Available at: https://www.hindawi.com/journals/jnm/2011/348268/ (Accessed: 9 February 2011).

Sun, J., Wang, B., Liu, Y., Zhang, L., Ma, A., Yang, Z., Ji, Y. and Liu, Y. (2014) *Transcription factor KLF9 suppresses the growth of hepatocellular carcinoma cells in vivo and positively regulates p53 expression*, Cancer Letters, 355(1), pp. 25–33.

Szot, C. S., Buchanan, C. F., Freeman, J. W. and Rylander, M. N. (2011) *3D in vitro bioengineered tumors based on collagen I hydrogels*, Biomaterials, 32(31), pp. 7905–7912.

Tabatabaei, F., Moharamzadeh, K. and Tayebi, L. (2020) *Fibroblast encapsulation in gelatin methacryloyl (GelMA) versus collagen hydrogel as substrates for oral mucosa tissue engineering,* Journal of Oral Biology and Craniofacial Research, 10(4), pp. 573–577.

Theise, N. D., Saxena, R., Portmann, B. C., Thung, S. N., Yee, H., Chiriboga, L., Kumar, A. and Crawford, J. M. (1999) *The canals of Hering and hepatic stem cells in humans*. Hepatology, 30(6), pp. 1425–1433.

Tsuchida, T. and Friedman, S. L. (2017) *Mechanisms of hepatic stellate cell activation*, Nature Reviews Gastroenterology and Hepatology, 14(7), pp. 397–411.

Walimbe, T. and Panitch, A. (2020) *Best of Both Hydrogel Worlds: Harnessing Bioactivity and Tunability by Incorporating Glycosaminoglycans in Collagen Hydrogels*, Bioengineering [Online]. Available at: https://pubmed.ncbi.nlm.nih.gov/33276506/ (Accessed: 2 December 2020).

Wang, X., Hassan, W., Zhao, J., Bakht, S., Nie, Y., Wang, Y., Pang, Q. and Huang, Z. (2019) *The impact of hepatocyte nuclear factor-1α on liver malignancies and cell stemness with metabolic consequences*, Stem Cell Research and Therapy [Online]. Available at: https://www.ncbi.nlm.nih.gov/pmc/articles/PMC6829964/ (Accessed: 4 November 2019).

Wilkinson, D., Alva-Ornelas, J., Sucre, J., Vijayaraj, P., Durra, Abdo, Richardson, W., Jonas, S., Paul, M., Karumbayaram, S., Dunn, B., Gomperts, B. (2016). Tissue Engineering and Regenerative Medicine TISSUE ENGINEERING AND REGENERATIVE MEDICINE Concise Review: The Potential Use of Intestinal Stem Cells to Treat Patients with Intestinal Failure. *Stem Cells Translational Medicine*, 6(2), pp. 666–676.

World Health Organization. (2020) *Cancer Country Profile 2020*, International Agency for Research on Cancer [Online]. Available at:

https://www.who.int/cancer/country-profiles/TUR_2020.pdf (Accessed: 1 January 2020).

Yang, S., Koteish, A., Lin, H., Huang, J., Roskams, T., Dawson, V. and Diehl, A. M. (2004) *Oval Cells Compensate for Damage and Replicative Senescence of Mature Hepatocytes in Mice with Fatty Liver Disease*, Hepatology, 39(2), pp. 403–411.

Yoon No, D., Lee, K. H., Lee, J. and Lee, S. H. (2015) *3D liver models on a microplatform: well-defined culture, engineering of liver tissue and liver-on-a-chip*, Lab on a Chip, 15(19), pp. 3822–3837.

Zhou, L., Hinerman, J. M., Blaszczyk, M., Miller, J. L. C., Conrady, D. G., Barrow, A. D., Chirgadze, D. Y., Bihan, D., Farndale, R. W. and Herr, A. B. (2016) *Structural basis for collagen recognition by the immune receptor OSCAR*, Blood, 127(5), pp. 529-537.

Sepmag. (2022) *Cell Lysis Buffer,* [Online]. Available at: https://www.sepmag.eu/blog/cell-lysis-buffer (Accessed: 26 August 2022).